Cancer Letters 637 (2026) 218131



Contents lists available at ScienceDirect

Cancer Letters

journal homepage: www.elsevier.com/locate/canlet



Original Articles



Drug screening reveals differential drug response in primary and metastatic clear cell sarcoma

Djenana Vejzovic [a], Christina Karner [a], Karoline Fechter [b], Gerald Ritter [b], Viktoria Holzer [a], Lisa Barones [b], Nina A. Schweintzger [c,d], Karin Wagner [c], Freya Lyssy [e], Martin Gauster [e], Joanna Szkandera [f], Stefanie Stanzer [f,g], Barbara Prietl [g,j], Amin El-Heliebi [e], Birgit Lohberger [h], Maria Jose Guillén-Navaro [i], Pablo M. Avilés [i], Iva Brčić [a], Bernadette Liegl-Atzwanger [a], Beate Rinner [a,k,*]

[a] Diagnostic and Research Institute of Pathology, Medical University of Graz, Graz, Austria
[b] Division of Biomedical Research, Medical University of Graz, Graz, Austria
[c] Center for Medical Research, Medical University of Graz, Graz, Austria
[d] Division of General Pediatrics, Department of Pediatrics and Adolescent Medicine, Medical University of Graz, Austria
[e] Division of Cell Biology, Histology and Embryology, Gottfried Schatz Research Center, Medical University of Graz, Austria
[f] Division of Clinical Oncology, Department of Medicine, Medical University of Graz, Graz, Austria
[g] Center for Biomarker Research in Medicine (CBmed), Graz, Austria
[h] Department of Orthopedics and Trauma, Medical University of Graz, Graz, Austria
[i] PharmaMar, Madrid, Spain
[j] Division of Endocrinology and Diabetology, Department of Internal Medicine, Medical University of Graz, Graz, Austria
[k] BioTechMed-Graz, Graz, Austria

A B S T R A C T

Clear Cell Sarcoma (CCS) are ultra-rare fusion-translocated soft-tissue tumours occurring mainly in young adults with poor prognosis. Their aggressiveness and resistance to conventional chemotherapy, especially in a metastatic setting, characterize these tumours. A functional drug screen consisting of 80 drugs was performed on patient-derived CCS cell lines. Top candidates were validated in 3D cell culture and in vivo models, allowing comparison of drug responses among CCS cell lines, including one matched pair (MUG Lucifer cell lines) representing primary and metastatic disease from the same patient. Underlying mechanisms were evaluated with RNA Seq, fluorescence/luminescence based assays, Western blot and IHC. *In vitro* experiments in CCS spheroids highlighted the transcription inhibitor lurbinectedin to be the best overall candidate which was further confirmed in mouse xenografts, albeit to a lesser extent than observed in vitro, especially in the metastatic CCS model. Transcriptional and functional analyses revealed heterogeneous drug responses and differences in cell death mechanisms across CCS lines, reflecting patient-specific variability. Furthermore, we explored combination treatment of lurbinectedin with selinexor. Synergistic effects were confirmed in a novel autologous co-culture model incorporating cancer-associated fibroblasts, providing a more physiologically relevant system for drug testing. This study identified promising therapeutic avenues by highlighting key vulnerabilities in CCS, considering both inter-tumour heterogeneity, tumour plasticity and the stromal influence on drug response.

1. Introduction

Soft-tissue sarcomas are rare mesenchymal malignancies [1]. The limited number of cases, diverse histopathological features, variations in anatomical localization and biological behaviour pose a considerable challenge to a comprehensive understanding of this disease, resulting in a dismal prognosis with a median overall survival of between 12 and 15 months in patients with advanced disease (locally advanced or metastatic) [2,3].

Clear cell sarcoma (CCS) is an *ultra-rare* sarcoma subtype (incidence 1:100,000,000) with high rates of recurrence and metastasis characterized by gene fusions most commonly affecting the *EWSR1* gene and the transcription factor *ATF1* [4,5]. The diagnosis of CCS is made by a combination of morphology, immunohistochemistry and fusion analysis. CCS expresses melanocytic markers like SOX10, S100, HMB45 and Melan-A, but in contrast to melanomas CCS demonstrates fusions

Abbreviations: CCS, clear cell sarcoma; CAF, cancer-associated fibroblasts; NHDF, normal human dermal fibroblasts; TME, tumour microenvironment.

* Corresponding author. Diagnostic and Research Institute of Pathology, Medical University of Graz, Neue Stiftingtalstraße 6, 8010 Graz, Austria.
E-mail address: beate.rinner@medunigraz.at (B. Rinner).

https://doi.org/10.1016/j.canlet.2025.218131
Received 30 December 2024; Received in revised form 30 October 2025; Accepted 9 November 2025
Available online 11 November 2025
0304-3835/© 2025 The Authors. Published by Elsevier B.V. This is an open access article under the CC BY license (http://creativecommons.org/licenses/by/4.0/).

involving the *EWSR1* or *FUS* gene with ATF1, *CREB1 or CREM* [6]. The fusion in the context of morphology and immunohistochemistry is the defining cytogenetic abnormality and CCS usually lacks other recurrent large scale genetic alterations. Treatment options for CCS are limited with wide resection of the primary tumour still being the gold standard. Systemic therapy is predominantly required for metastatic and/or unresectable disease, with first-line therapy consisting mainly of the anthracycline-based treatment (e.g. doxorubicin), followed by alkylators like ifosfamide as a second-line agent [7]. This soft-tissue sarcoma treatment regime has limited benefit for CCS emphasizing the urgent need for new therapeutic strategies beyond the conventional approach [8].

Modern precision oncology approaches heavily focus on matching treatments based on the molecular profile or defined treatment targets, but especially for solid tumours, this has been inefficient potentially attributable to oversimplified models that fail to encompass the complexity of the tumour microenvironment (TME) or account for metastatic cell plasticity [9–12]. Numerous studies, on the other hand, have indicated that functional drug testing yields superior clinical outcomes by identifying potential vulnerabilities independent of molecular characteristics or gene variants that might otherwise go unnoticed [13–16].

We recently reported the establishment and characterization of our novel CCS cell lines: one derived from the primary tumour, MUG Lucifer prim, and one from the metastatic lesion, MUG Lucifer met [17]. In the current study, we aimed to identify new potential candidates for treating CCS through a functional drug screening of 80 FDA approved drugs. We selected a panel of four CCS cell lines, including our self-established MUG Lucifer cell lines for evaluation. Based on comprehensive validation in 3D patient-derived spheroids and xenografts, we provide a novel therapeutic strategy defined by inhibition of oncogenic transcription. In addition, we found differences in transcriptomic signatures between primary and metastatic CCS and created a novel complex 3D multicellular model for basic and translational research considering the tumour microenvironment and involving cellular plasticity of metastatic cells. In summary, this study illustrates a promising new approach for metastatic and advanced clear cell sarcoma (CCS). By combining patient-derived models, functional drug screening, and transcriptomic analyses, we not only identified lurbinectedin as a potential targeted agent, but also revealed substantial differences between primary and metastatic CCS in terms of drug response and underlying biology. These findings highlight the need to consider distinct therapeutic strategies depending on disease stage and site, rather than applying a one-size-fits-all treatment approach. Our work underscores the importance of tailored therapy design for CCS and establishes a valuable platform for future translational research in this ultra-rare cancer type.

2. Materials and methods

2.1. Cell culture

For all experiments, clear cell sarcoma cell lines MUG Lucifer prim and MUG Lucifer met were used. Both cell lines were established and characterized in our previous publication [17]. Briefly, MUG Lucifer prim was established from a primary tumour in the knee and MUG Lucifer met from the metastatic lesion in the lung of the same CCS patient. Furthermore, two other clear cell sarcoma cell lines, CCS24 and CCS210, were used for all experiments for additional validation. CCS24 and CCS210 were a kind gift from Jonathan A. Fletcher, Brigham And Women's Hospital, Boston, Massachusetts, USA. Immortalized normal dermal skin fibroblasts (hTERT MUG Lucifer NHDF) from the same patient as both MUG Lucifer tumour cell lines were isolated from a piece of healthy skin and immortalized by lentiviral transduction of the hTERT gene, which were used as a healthy control in selected experiments. CAF of tumour cells were obtained from cultures frozen away during the establishment of the cell line, which still contained parts of non-malignant cells. The cells were separated by trypsinization and different densities. After obtaining pure CAF cultures, immortalization was performed using hTERT as described in the previous publication [17]. A detailed description of the establishment process, including characterization steps, is provided in the supplementary material. All CCS cell lines and the MUG Lucifer hTERT CAF were cultivated in DMEM/F-12 (Gibco, Life Technologies, Germany) supplemented with 10 % fetal bovine serum (FBS) (Gibco), 2 mM L-Glutamine and Pen Strep (100 Units/ml Penicillin and 100 µg/ml Streptomyin, Gibco). For hTERT MUG Lucifer NHDF DMEM (Gibco) with the same supplements was used. Cells were kept in a humidified 5 % CO_2 atmosphere at 37 °C. The p53 mutation status of MUG Lucifer cell lines was determined using the TP53 amplicon panel (Next-Generation Sequencing) as part of routine testing conducted by the Diagnostic and Research Institute of Pathology, Medical University of Graz.

For lurbinectedin efficacy screening across cell lines, the following cell lines were used: the EWSR1-fusion-associated sarcoma cell lines MUG Lucifer prim, MUG Lucifer met, SK-ES-1 (Ewing sarcoma), and MHH-ES-1 (Ewing sarcoma); the non-EWSR1-fusion-associated sarcoma cell lines TE-671 (rhabdomyosarcoma), SW-872 (liposarcoma), SW-1353 (chondrosarcoma), SW-684 (fibrosarcoma), U2-OS (osteosarcoma), and SW-982 (synovial sarcoma); and the non-sarcoma cell lines A549 (lung cancer), MCF-7 (breast cancer), A375 (malignant melanoma), and ESO-51 (esophageal adenocarcinoma). SK-ES-1 were cultivated in McCoy's 5a media (Gibco) supplemented with 1.5 mM L-Glutamine and 15 % FBS. SW-684, SW872, SW-982, MCF-7 and A549 were cultivated in DMEM/F-12 supplemented with 10 % FBS, 2 mM L-Glutamine and Pen Strep. TE-671, SW-1353, A375 and U2-OS were cultivated in DMEM supplemented with 10 %FBS, 2 mM L-Glutamine and 1 % Pen Strep. ESO-51 and MHH-ES-1 were cultivated in RPMI (Gibco) supplemented with 10 % FBS, 2 mM L-Glutamine and 1 % Pen Strep. All experiments were performed with mycoplasma-free cells. All cells were regularly authenticated by short tandem repeat analysis using the commercially available Power Plex® 16 HS System (Promega Corporation, Germany) according to protocol.

2.2. Drug screening

The drug panel for the tumour cell line screen consisted of 80 anticancer agents reconstituted in DMSO at a stock solution of 10 mM. For the drug screening of the fibroblasts cell lines, a new panel consisting of only 37 agents was used. The used clinical and preclinical drugs include e.g. receptor tyrosine kinase inhibitors (targets e.g.: EGFR, PI3K/AKT/mTOR pathway, PDGFR), inhibitors of the proteasome, hedgehog-signaling inhibitors etc. All drug compounds were purchased from MedChemExpress and Eubio. Cells were treated with drugs in a seven-point serial dilution series (20 µM–4.88 nM; exceptions: lurbinectedin and gilteritinib hemifumerate 66,667 nM to 66,667 nM and temozolomide 500 nM to 0,122 nM) using the Echo 650 Liquid Handler (Beckmann Coulter) in duplicates. Each plate included seven positive controls (bortezomib; 5 µM) and seven vehicle controls (dimethyl sulfoxide (=DMSO); 0.5 %). The drug screening layout was created using the Echo Dose-Response software (Beckman Coulter, USA).

After two days of incubation at 37 °C in a 5 % CO_2 humidified standard incubator cell viability was assessed using an adenosine triphosphate (ATP) monitoring system based on luciferase and assessed by an EnVision Multilabel Reader (PerkinElmer, USA). Briefly, for readout, intracellular ATP levels, which serve as a surrogate for cell viability, were measured using the CellTiter-Glo (Promega) reagent. After addition of 10 µl (1:5) of the CellTiter-Glo reagent using a MultiFlo FX Multimode dispenser (BioTek, USA), the culture plate was incubated to allow lysis of the cells. Readout was performed by measuring the luminescence signal from each individual well by using an EnVision Multilabel Reader (PerkinElmer). For the lurbinectedin efficacy screening, 1250 cells were seeded per well in black, clear-bottom, ultra-low attachment spheroid 384-well culture plates (Corning, USA) for

each cell line and treated with lurbinectedin (0–4 nM, four-fold dilutions). The cells were incubated for 48 h, following the same protocol as the other assays. Readout and analysis were performed analogously to all viability assays.

2.3. Data processing and quality controls

Quality control measures included the calculation of the mean, standard deviation (SD), and coefficient of variation (CV) of the luminescence signal from the negative controls. The cutoff for the CV was set to 30 % [18]. The Z′ factor was calculated on every single plate to evaluate the degree of overlap between the mean of the negative control (n = 7 per plate) and the mean of the positive control (n = 7 per plate). These Z′ factor indicates the quality of the data generated in the screening plate to evaluate whether the specific cellular feature was suitable as a statistically robust assay readout. The Z′ factor values were categorized as follows: Z′ = 0.5 to 1 excellent, 0 to 0.5 acceptable, and <0 unacceptable due to too much overlap between positive and negative controls. For data analysis, the signal obtained from the negative control wells were used to calculate the relative cell viability and to normalize the data on a per-plate basis. In brief, the signals obtained from these wells was set to 100 % and the relative viability per well per drug was calculated. Dose response curve (DRC) fitting per drug was performed using GraphPad Prism X (GraphPad) and the Area under the curve (AUC) was evaluated. Best-fitting lines were calculated using GraphPad: [log(inhibitor) vs. response − variable slope (four parameters)]. $Y = \text{Bottom} + (\text{Top} - \text{Bottom})/(1 + 10\hat{}((\log IC50 - X) \times \text{HillSlope}))$. The AUC of each curve was determined using GraphPad Prism X.

2.4. Selected drugs

2.4.1. Cell viability assay in 3D cell culture

To evaluate the anti-tumour activity of selected drugs (selinexor, panobinostat and lurbinectedin) on the cell viability of CCS cell lines the commercially available CellTiter-Glo® 3D Cell Viability Assay (Promega, Germany) was performed according to manufacturer's protocol. The ATP based assay determines cell viability in 3D spheroids by quantification of bioluminescent readouts. 2.5×10^3 cells were seeded in clear, round bottom ultra-low attachment plates (ULA) and incubated overnight at 37 °C in a 5 % CO_2 atmosphere. After 24h incubation cells were treated with selinexor, panobinostat and lurbinectedin in increasing concentrations and incubated again for 48 h. Lysed spheroids were then transferred in white opaque plates and cell viabilities were measured on a CLARIOstar microplate reader (BMG Labtech, Ortenberg, Germany). DMSO served as a vehicle control. Cell viabilities were normalized to vehicle control and IC_{50} values calculated using GraphPad Prism.

2.4.2. Assessment of cell death in 3D spheroids

For time dependent analysis of cell death inducing effects on the CCS cell lines the commercially available multiplex RealTime-Glo™ Annexin V Apoptosis Necrosis Assay (Promega, Germany) was used. Cells were seeded 2.5×10^3 per well in black with clear round bottom, ULA, 96-well plates (Corning) and incubated overnight. Yielding spheroids were then treated with 81 nM selinexor, 2.1 nM panobinstat and 0.05 nM lurbinectedin, each being the previously calculated IC_{50} values for MUG Lucifer prim. To the treated cells, 100 µl of 2X RealTime-Glo™ Annexin V Apoptosis Necrosis detection reagent was added to each well and afterwards measured for 48 h with the CLARIOstar microplate reader. DMSO served as a vehicle control and was used as a baseline for analysis. All signal values were blank (media only, no cells) adjusted before actual analysis. After the 48-h incubation, endpoint caspase-3/7 activities were measured as luminescent signals in the same plate by addition of the commercially available Caspase-Glo 3/7® Assay Reagent (Promega) according to the protocol provided by the manufacturer.

2.4.3. Combination treatments

For synergy evaluation $0.5–1 \times 10^4$ cells were seeded into white, flat-bottom, 96-well plates (Corning). Twenty four hours later, selinexor and/or lurbinectedin were added, and viability was assessed after 48 h analogously to the drug screening. Viabilities were normalized to the vehicle control (DMSO) and synergistic interactions evaluated using SynergyFinder 3.0 according to the Bliss, ZIP, HSA and Loewe algorithm [19]. For validation in multicellular spheroids, tumour cells (MUG Lucifer prim, MUG Lucifer met) were co-cultured with hTERT MUG Lucifer CAF (ratios: 1 + 1, 1 + 4) in ULA plates and left to form spheroids overnight analogously to the tumour single cultures and treated in a range of the previously determined IC_{50} values and 10 x IC_{50}.

2.4.4. RNA seq

Total RNA extraction from cell pellets was done with the miRNeasy Micro Kit (Qiagen, Hilden, Germany) including DNAse treatment with the RNase-Free DNase Set (Qiagen, Hilden, Germany). RNA quantity and quality were assessed using the NanoDrop 2000 Spectrophotometer (Thermo Fisher Scientific, Waltham, Massachusetts) and BioAnalyzer BA2100 (Agilent, Foster City, CA), respectively.

RNA-Seq libraries were generated using the NEBNext® Ultra™ II Directional RNA Library Prep Kit for Illumina® with the NEBNext® Poly (A) mRNA Magnetic Isolation Module (both from New England Biolabs, Frankfurt am Main, Germany), following manufacturer's instructions. Individual libraries were pooled equimolar and sequenced by the Next Generation Sequencing Facility at Vienna BioCenter Core Facilities (VBCF), Austria on an Illumina NextSeq550 with 75bp paired-end. The RNASeq analysis pipeline consisted of quality control using FastQC. MultiQC [20], alignment to Ensembl gene reference Homo sapiens GRCh38 and read counting using STAR [21], SAMtools [22] and FeatureCounts [23] in the Galaxy software suite. Normalized counts for each gene were calculated using DESeq2 (v1.34.0) [24] with default parameters. Genes with a read count of at least 10 over all rows were considered lowly expressed and were removed, leaving a total of 19,908 genes. The latter were considered to be differentially expressed when the adjusted p value (or false-discovery rate, FDR) was ≤0.05. P values were corrected for multiple testing with independent hypothesis weighting (IHW v1.22.0) [25] after Benjamini-Hochberg (BH). Volcano plots were used to visualize log2 fold-changes (LFC) and adjusted p-values (EnhancedVolcano v1.12.0). Genes that passed the adjusted p-value threshold of 0.05 and the absolute log2 fold-change threshold of 1 are shown in red. Dotted lines represent the thresholds. Lists of significantly differentially expressed genes were subjected to either KEGG pathway analysis or Gene Ontology terms using g-Profiler with tdefault parameters. Heat maps showing AUC values were generated with ComplexHeatmap v2.10.0 [26].

2.4.5. Immunoblotting

Whole cell protein extracts were prepared with lysis buffer (50 mM Tris-HCl pH 7.4, 150 mM NaCl, 1 mM NaF, 1 mM EDTA, 1 % NP-40, 1 mM Na3VO4) and a protease inhibitor cocktail (P8340; Sigma Aldrich), 24 h (pAkt and Akt) and 48h (rest) after treatment with 0, 0.05, 0.2, and 0.8 nM (MUG Lucifer prim.), respectively 0, 0.0125, 0.05, and 0.2 nM (MUG Lucifer met.) lurbinectedin. Protein concentration was determined with the Pierce BCA Protein Assay Kit (Thermo Fisher Scientific). The proteins were separated by SDS-PAGE and were blotted on Amersham™ Protran™ Premium 0.45 µM nitrocellulose membranes (GE Healthcare Life Science, Little Chalfont, UK). Primary antibodies against $p21^{Waf1/Cip1}$, p53, MDM2, GADD45A, phospho-AKT, AKT (all Cell Signaling Technology, Danvers, MA) and β-actin as loading control were used. Blots were developed using a horseradish peroxidase-conjugated secondary antibody (Dako) for 1h and the Amersham™ ECL™ prime western blotting detection reagent (GE Healthcare). Chemiluminescence signals were detected with the ChemiDocTouch Imaging System (BioRad Laboratories Inc, Hercules, CA) and images were processed with the ImageLab 5.2 Software (BioRad Laboratories Inc).

2.4.6. Animal experiments

For the first experiment, 60 six-week-old female athymic nude (Rj: ATHYM-Foxn1nu/nu) mice (Janvier Labs, Saint Berthevin, France) were housed under specific-pathogen-free (SPF) conditions in ventilated cages and fed ad libitum. After an acclimation period of two weeks, mice were randomly divided into two groups (MUG Lucifer prim xenograft and MUG Lucifer met xenograft, n = 30 per group). 5×10^6 cells in 100 µl PBS of each cell line were injected subcutaneously (s.c.) into the right posterior flank. Tumours started to grow for both groups after approximately seven days. Mice with excessively fast-growing tumours or that due to poor health did not receive three doses were excluded from the analysis, as no appropriate controls were available for comparison. An Excel file containing all mice, including time points and tumour volume measurements (both included and excluded animals), is provided in the supplementary materials. Mice were injected intravenously once a week with either 0.18 mg kg^{-1} lurbinectedin or placebo for a maximum of three weeks, based on the animal's state of health (s. Fig. 3A). Animals were sacrificed after reaching the previously established termination criteria (general poor health, more than 20 % weight loss, tumour larger than 1000 mm^3). For the second experiment, six mice per cell line were injected as in the first experiment and, after tumour establishment, divided into two groups (n = 3 per condition). The treatment and placebo groups were matched to have nearly identical tumour size distributions, with slightly larger tumours deliberately assigned to the treatment group to avoid bias regarding growth behavior. All mice received treatment on the same day and were harvested on the same day to enable direct comparison of tumour sizes and growth curves.

Tumour growth was monitored at least once a week by high-frequency ultrasound imaging (HF-US). Cell injection and HF-US were performed under anesthesia with a constant administration of 1.5–2 % isoflurane in a permanent airflow of 1.5 L per minute. Afterwards, histopathological examination and blood analyses by using V-Sight hematology analyzer (A. Menarini GmbH, Vienna, Austria) were performed. Tissues (organs and tumour) were fixed in 4 % paraformaldehyde solution for 24 h and embedded in paraffin. All of the animal work complies with the ARRIVE guidelines and has been approved by the committee for institutional animal care and use at the Austrian Federal Ministry of Science and Research (BMWFW) (vote 66.010/0046-WF/V/3b/2016 amendment GZ 2023–0.288.358). We used the ARRIVE checklist when writing our report [27].

2.4.7. Ultrasound imaging

Tumour growth was monitored once a week by using a Vevo3100 HF-US system quipped with transducers ranging from 24 to 70 MHz (Fujifilm VisualSonics, Inc., Toronto, ON, Canada). Sagittal and transversal images of the region of interest were obtained. Calculation of tumour volume was performed with VevoLab Software (Version 5.5.1, Fujifilm VisualSonics Inc.) using the formula Volume (mm^3) = [3.141 x length (mm) x width (mm) x depth (mm)]/6. 3D und Power Doppler mode was used to calculate percent vascularity of the tumours.

2.4.8. Immunohistochemistry

FFPE of tissues (organs and tumour) were fixed in 4 % paraformaldehyde solution for at least 24 h and embedded in paraffin. All samples were stained at the Diagnostic and Research Institute of Pathology of the Medical University of Graz.

Spheroids were fixed directly in wells with 4 % formaldehyde (Diapath S.p.A., Martinengo BG, Italy) for 30 min, before three wash steps with PBS (Gibco). During the last wash step, up to four spheroids were pooled and transferred into an Eppendorf tube to undergo manual paraffin embedding steps. Blocks were cut into 5 µm sections and mounted onto Superfrost Plus slides (Thermo Fisher Scientific). After deparaffinization, slides were stained for H&E as previously described [28]. In brief, spheroid sections were incubated in acid hemalaun according to Mayer (Hematoxylin monohydrate, Merck) for 10 min. To change the pH-value, sections were then incubated shortly in 1 % ammonia solution (Merck, Germany), followed by a 1 min incubation step in 1 % aqueous eosin (Eosin Y (yellowish), (Sigma Aldrich) before slides were permanently mounted with Cytoseal (Glas™ Tissue Mount™, Tissue-Tek®, Sakura Finetek Germany GmbH, Umkirch, Germany) and a cover slip. Images were obtained with an Evident Olympus VS200 Slide Scanner (Evident Corpotation, Tokyo, Japan). For immunohistochemistry, spheroids were stained with antibodies for SOX-10, Melan-A, HMB45, α-SMA (all Dako, USA) and Tenascin C (Origene, Rockville, USA).

2.5. Statistical analysis

Details of statistical tests for each experiment can be found in the respective figure legends including normality testing if applicable. All in vitro data are displayed as mean ± SEM based on three independent experiments unless otherwise stated. Prism7 (GraphPad, San Diego, CA, USA) was used for all statistical analysis. For mouse experiments, all animals were included in the analysis, unless no tumour growth was observed (in the case of two mice of MUG Lucifer met). No statistical method was employed to determine the sample size; rather, group sizes were decided based on findings from preliminary experiments and laboratory experience. Groups were randomly allocated for tumour injection and then based on tumour size for treatment start and data analysis (tumour growth, survival). The investigators were not blinded to allocation during outcome assessment; however pathologists were blinded during necrosis estimation.

3. Results

3.1. Drug screening of 80 selected compounds identifies potential vulnerabilities in CCS

A panel of four patient-derived CCS cell lines (MUG Lucifer prim, MUG Lucifer met, CCS24, and CCS210) was screened using a single-agent library of 80 FDA approved chemotherapeutics and targeted drugs covering a broad range of targets associated with well-known cancer pathways such as e.g., epidermal growth factor receptor (EGFR), hepatocyte growth factor receptor (MET), anaplastic lymphoma kinase (ALK) or phosphoinositide 3-kinase (PI3K) (Table S1, Fig. 1a). All drugs are already approved and in use for the treatment of other cancer types (for instance multiple myeloma, non-small cell lung cancer etc.) enabling a faster translation into the clinic due to already investigated safety profiles [18,29]. Cell lines treated with this library generated dose-responses, which built the basis of analyzing both efficacy and potency of these agents in decreasing cell viability of CCS. We decided to use two different sensitivity measure, focusing primarily on the area under the curve (AUC) and the half maximal inhibitory concentration (IC_{50}) to classify response of each tested drug. To do so, we first calculated area under the curve (AUC) values of each drug response, yielding in a total of 320 obtained AUC values. Furthermore, AUC values less than 200 in all four cell lines were regarded as "sensitive", whereas values above as "resistant" (Fig. 1b). Only five agents (lurbinectedin, panobinostat, bortezomib, carfilzomib, ixazomib) out of 80 (6.3 %) classified as "sensitive", whereas 43 drugs (53.8 %) did not show any effect on the four tested cell lines. Not surprisingly, the "resistant" cluster revealed, that, none of the cell lines responded to conventional cytostatics such as irinotecan or oxaliplatin. Noteworthy, none of the tested cell lines demonstrated susceptibility to any of the Hedgehog pathway inhibitors and most of the PI3K inhibitors evaluated (Fig. S1a). On the other hand, the "sensitive" category revealed proteasome, transcription and HDAC inhibitors to be among the most potent and efficient drugs against CCS based on their AUC values revealing potential vulnerabilities for the disease (Fig. 1b and Fig. S1b–g). Especially, the transcription inhibitor lurbinectedin showed subnanomolar activity in all cell lines tested. Ecteinascidins, like lurbinectedin, are reported to especially inhibit transcriptionally driven tumours such as translocation-associated sarcomas, by suppressing

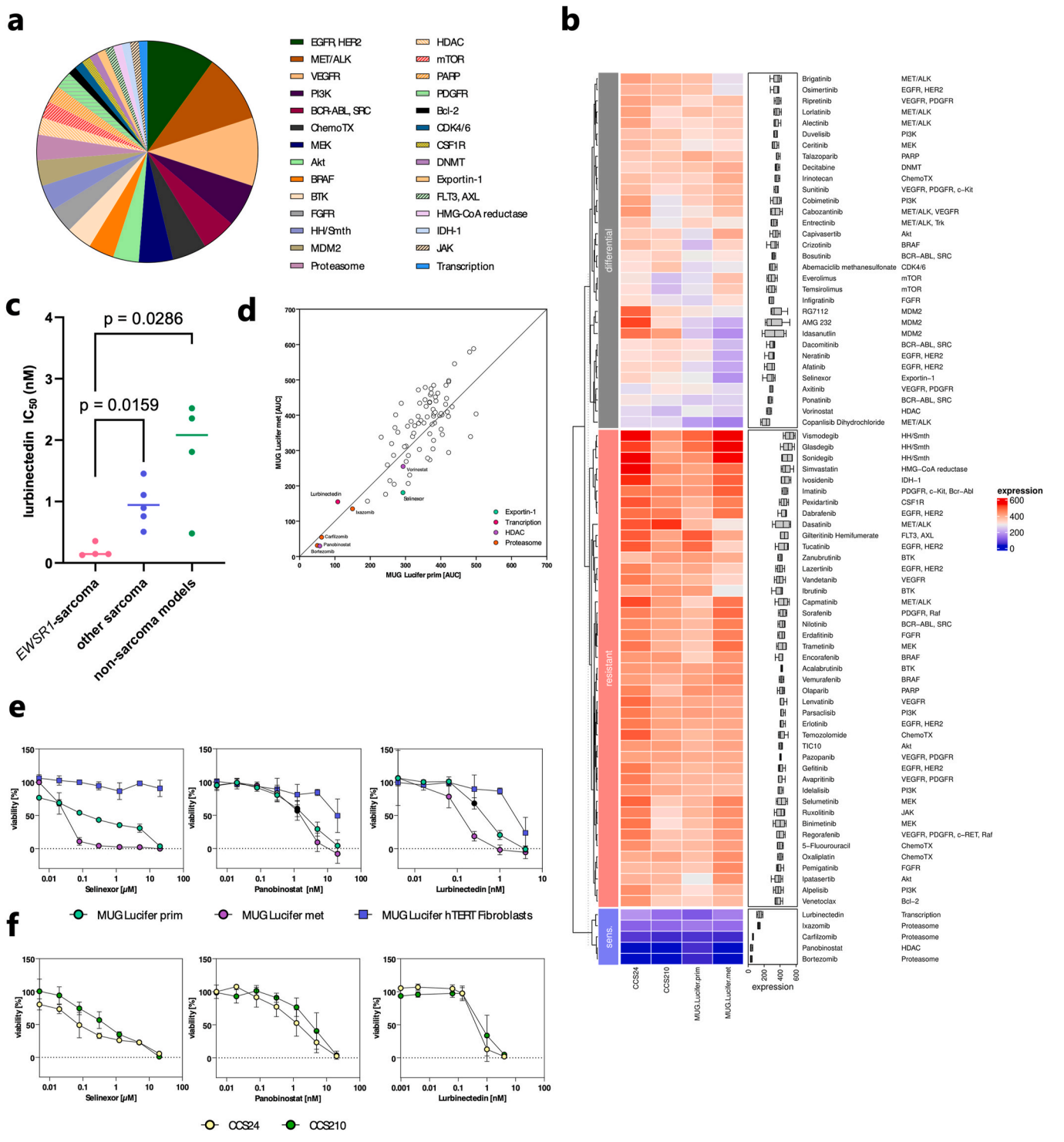

Fig. 1. High-throughtput drug screening reveals lead compounds against CCS

(**a**) Pie chart depicting target group distribution used in the functional drug screening (**b**) Heat map portraying AUC values for compounds tested on four patient-derived clear cell sarcoma cell lines including the self-established matched primary and metastatic MUG Lucifer cell lines from the same patient. AUC values below 200 in all cell lines were regarded as "sensitive", whereas above as "resistant". (**c**) Comparison of IC50 values was based on dose-response curves generated using CellTiter-Glo for 14 different cell lines, including *EWSR1*-fusion sarcoma, non-*EWSR1*-fusion sarcoma, and non-sarcoma models. IC_{50} values were calculated using dose-response curves in GraphPad Prism. Normality was formally tested using the Shapiro-Wilk test and was not fulfilled. Therefore, the Mann-Whitney *U* test was used to statistically compare results. P-values below 0.05 were considered significant. (**d**) Scatter plot describing drug sensitivities between primary and metastatic CCS reveals top metastatic favoring compounds to be selinexor, panobinostat and bortezomib, with significantly lower AUC values in the metastatic cell line, portraying selective compounds for this particular phenotype. **(e)** Dose response for selinexor, panobinostat and lurbinectedin treated CCS spheroids. For IC_{50} determination, dose response curves were generated using GraphPad Prism. MUG Lucifer cells (primary tumour, metastasis and healthy fibroblasts) were summarized in one graph for better comparability and elucidation of the model system. (**f**) Dose response for selinexor, panobinostat and lurbinectedin for cell lines CCS24 and CCS210, representative of two additional donors. Results for dose responses are represented as mean ± SEM of three individual experiments of at least three technical replicates.

super-enhancer-driven transcription [30]. In light of this, we further explored the sensitivity of CCS (clear cell sarcoma) to lurbinectedin in comparison with other tumour types. We conducted a drug screen across 14 cell lines, including both sarcoma models (*EWSR1*-fusion positive and EWSR1-fusion negative) and non-sarcoma models (breast, lung, esophagus, skin). Our results revealed that *EWSR1*-fusion-positive sarcomas exhibited significantly lower IC_{50} values for lurbinectedin compared to other sarcoma and non-sarcoma models (Fig. 1c, Fig. S2A–C). For the remaining agents, we observed an ambiguous effect on the various cell lines, where no clear trend could be determined, which we categorized as "differential". In this category we determined a substantial amount of differences in drug sensitivities between the two cell lines "MUG Lucifer prim" and "MUG Lucifer met", which were both derived from the same patient but portray different phenotypes (primary vs. metastatic lesion) and differ in aggressiveness. To highlight these differences in drug response we compared AUC values for each drug of the respective cell lines yielding in a scatter plot (Fig. 1d). Again, the proteasome and HDAC inhibitors ranked top of the list clustering in the bottom left corner, with panobinstat and bortezomib being among the best performers of their respective groups with the overall lowest IC_{50} (Fig. S1B–E). In addition, the inhibitor of nuclear export, selinexor, performed selectively better in MUG Lucifer met compared to the other cell lines with a significantly lower IC_{50} (Fig. S1F).

Interestingly, out of all cell lines only MUG Lucifer prim was sensitive to crizotinib, an inhibitor of the MET/ALK tyrosine kinases and the only targeted therapy currently available for CCS at the moment, whereas its metastatic counterpart was resistant according to our classification. This is consistent with our previously reported results and the fact that the CCS patient from whom these cell lines were derived received crizotinib after the primary tumour had already been excised, representing the acquired resistance that occurred in vivo [17].

Based on these results, we selected the best candidate from each group, namely panobinostat, bortezomib and lurbinectedin for further validation of their efficacy. Additionally, we also incorporated selinexor into our validation cohort, recognizing its targeted efficacy against a particularly aggressive variant of CCS.

3.2. Key candidates demonstrate efficacy in CCS spheroids

Following drug screening analysis, we used the previously defined potential key candidates for further in-depth evaluation and validation of their efficacy against CCS in vitro in more advanced cell culture models. The representative candidates were tested on 3D tumour spheroids of the same cell lines used in the drug screening, and the obtained results compared to the initial drug screening. To determine IC_{50} concentrations, we generated 3D spheroids and treated again in the same concentration range determining the respective IC_{50} concentrations for 3D cell culture (Fig. 1d and e, Table 1). Out of all compounds, lurbinectedin presented the overall lowest IC_{50} concentrations in a sub-nanomolar range in all four tested cell lines (Table 1).

In contrast to the initial screening, in 3D spheroids, lower concentrations of lurbinectedin were necessary for MUG Lucifer met compared to MUG Lucifer prim to decrease cell viability. As we were not able to reproduce the results for bortezomib in 3D cell culture, we decided to not use it for further experiments (data not shown). In addition, we also tested every top candidate on MUG Lucifer hTERT NHDF, a normal immortalized fibroblast cell line from the MUG Lucifer CCS patient, to identify cytotoxic effects on normal, non-malignant cells. Selinexor did not have any effect on cell viability in the tested range, however, lurbinectedin and panobinostat decreased cell viability at higher concentrations (Fig. 1d).

Table 1
IC_{50} values of selected key candidates.

	IC_{50} values (nM)		
cell line	Selinexor	Panobinstat	Lurbinectedin
MUG Lucifer prim	81 ± 6	2.1 ± 0.9	0.5 ± 0.1
MUG Lucifer met	36 ± 7	1.7 ± 0.7	0.1 ± 0.03
CCS24	20 ± 0.09	1.9 ± 1.3	0.9 ± 0.6
CCS210	42 ± 0.1	4.9 ± 2.7	0.6 ± 0.2

IC_{50} values were determined for 3D cell culture of the four clear cell sarcoma cell lines.

Because metastatic cells possess the ability to evade cell death mechanisms, our objective was to assess whether the identified candidates could induce cell death or solely reduce cell viability [31]. Our focus was on the MUG Lucifer model, allowing us to discern disparities between primary and metastatic CCS directly.

For this purpose, commercially available kits were multiplexed and monitored over 48h yielding data about early apoptosis, secondary necrosis and caspase 3/7 activities. For better comparability between the cell lines, cells were treated with the MUG Lucifer prim IC_{50} value (for 3D cell culture) of each compound. Because all three assays were multiplexed in the same plate, we were able to directly compare them with each other, yielding in a timeline of cell death events.

Lurbinectedin induced in MUG Lucifer prim a significant increase in apoptotic signal starting after approximately 8h, finishing with secondary necrosis (Fig. 2a). In MUG Lucifer met, apoptotic signal started increasing after 6h, but promptly declined with the onset of increased necrotic signals (Fig. 2b). After 48h on Lurbinectedin Caspase 3/7 were still significantly higher compared to the vehicle control for MUG Lucifer prim, but not in the metastatic counterpart, despite using the same concentration (Fig. 2c).

Panobinostat did not increase luminescent or fluorescent signals in 48 h in any cell line tested (Fig. 2d and e). Also, no significant changes in caspase 3/7 activity could be determined in treated cells compared to the vehicle control (Fig. 2f). For selinexor, similar results were obtained as for lurbinectedin in MUG Lucifer met, however apoptotic and necrotic signals started increasing simultaneously in MUG Lucifer prim and no increase in Caspase 3/7 levels was detected (Fig. 2g–i). As a control, we performed the same assay on MUG Lucifer hTERT NHDF. Again, no effects could be detected for any of the three candidates on normal fibroblasts using the same concentrations (Fig. 2c–f, i-l).

3.3. Lurbinectedin decreases tumour growth in primary but not in metastatic xenografts

To assess translational potential of the gained in vitro data and to further investigate differences in drug response on primary and metastatic cells, we performed in vivo experiments with the best overall candidate, lurbinectedin. Human tumour cell lines injected subcutaneously into mice rarely metastasize and, to our best knowledge, no CCS metastasis mouse model exists, we thus again focused on our patient-derived cell lines MUG Lucifer prim and MUG Lucifer met for in vivo experiments in order to mimic CCS in an advanced stage. Both cell lines grow solid tumours when injected subcutaneously, but differ in their growth behavior with the metastasis derived cell line portraying a more aggressive model, which we also observed in our previous study [17]. Mice received three weekly doses of 0.18 mg kg^{-1} lurbinectedin intravenously [32,33]. Individual tumours have been tested for vascularization to ensure that lurbinectedin can enter the tumour via the vascular system, an example of which can be seen in Fig. S5K.

We began treatment once the mice developed visible tumours and monitored growth until tumours reached a tumour volume over 1000 mm^3 or until animals had to be euthanized according to approved ethical criteria, which allowed us to generate survival curves. Using this approach, we found that survival was significantly extended in both xenograft models, although the effect appeared more modest in the MUG Lucifer met model (Fig. 3a–b, Fig. S3A–B). To rule out the possibility that prolonged survival was simply a consequence of generally slower tumor growth of the placebo group, we repeated the experiment in a smaller cohort (n = 3 per condition). In this setup, groups were balanced

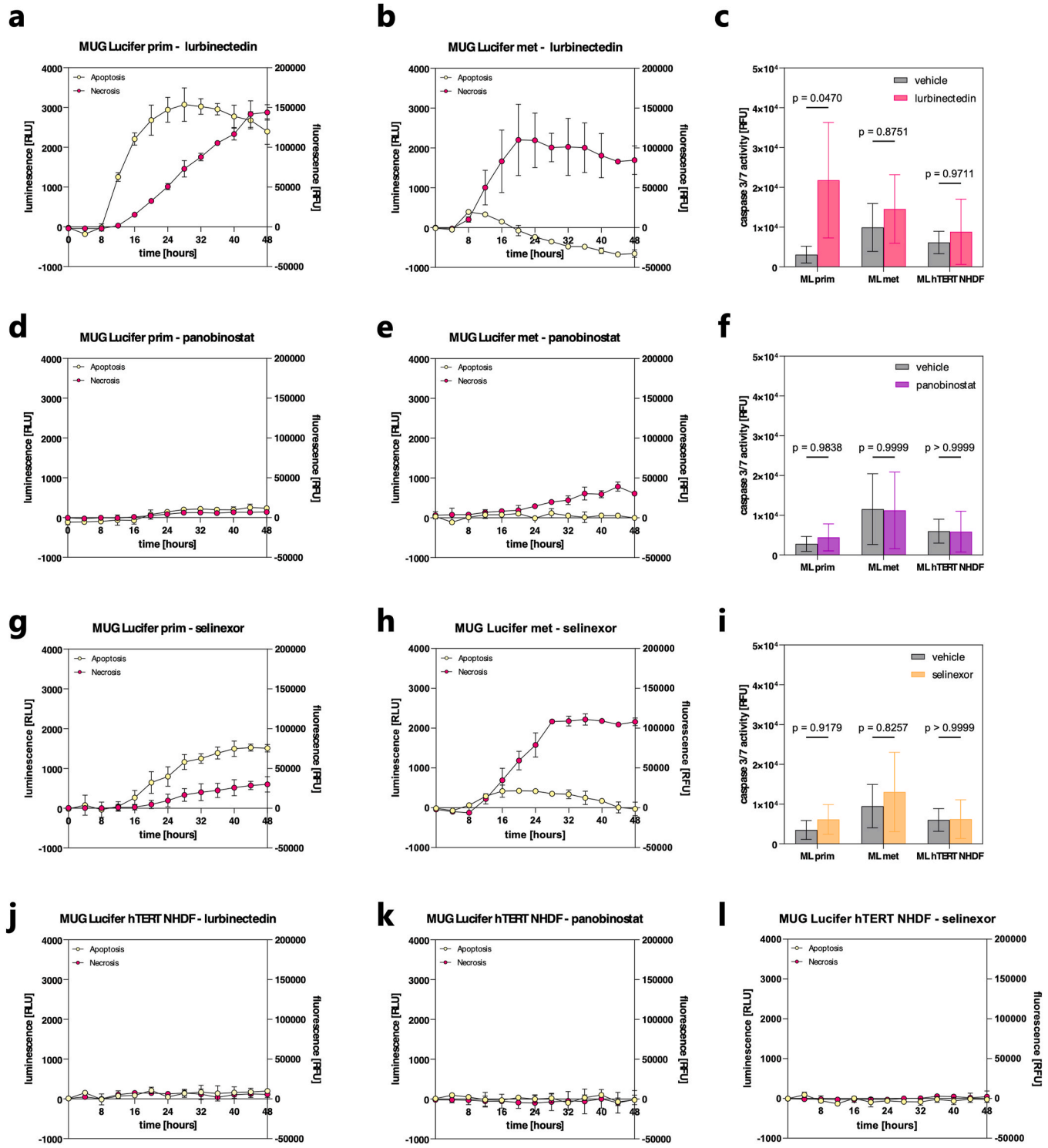

Fig. 2. Mode of in vitro cell death in tumour spheroids induced by lead compounds on MUG Lucifer cell lines
(**a-b**) Real-time assay monitoring apoptosis/necrosis upon lurbinectedin treatment for MUG Lucifer prim and MUG Lucifer met spheroids. Cells were treated with lurbinectedin IC_{50} concentrations for MUG Lucifer prim in both instances and monitored over 48h. DMSO monitored cells served as a baseline to normalize signal increase. (**c**) Caspase 3/7 levels as an endpoint measurement for 48h of MUG Lucifer prim (ML prim), MUG Lucifer met (ML met) and MUG Lucifer hTERT NHDF (ML hTERT NHDF) met were treated with lurbinectedin IC_{50} concentrations for MUG Lucifer prim for better comparability. (**d-e**) Real-time assays for panobinostat treated spheroids analogous to lurbinectedin (**f**) Caspase 3/7 levels after exposure to panobinostat analogous to lurbinectedin. (**g-h**) Real-time assays for selinexor treated spheroids analogous to lurbinectedin (**i**) Caspase 3/7 levels after exposure to selinexor analogous to lurbinectedin. (**j-l**) Real-time assays conducted on lurbinectedin, panobinostat and selinexor treated MUG Lucifer hTERT NHDF seving to identify cytotoxic effects on non-malignant cells induced by the respective compounds. Experiment was conducted in parallel to assays performed on tumour spheroids. Real time experiments were performed twice with three technical replicates each. Caspase 3/7 were performed as three independent experiments in at least duplicates. Data displayed as mean ± SEM. Two-way ANOVA was used for statistical analysis and p-values below 0.05 regarded as significant.

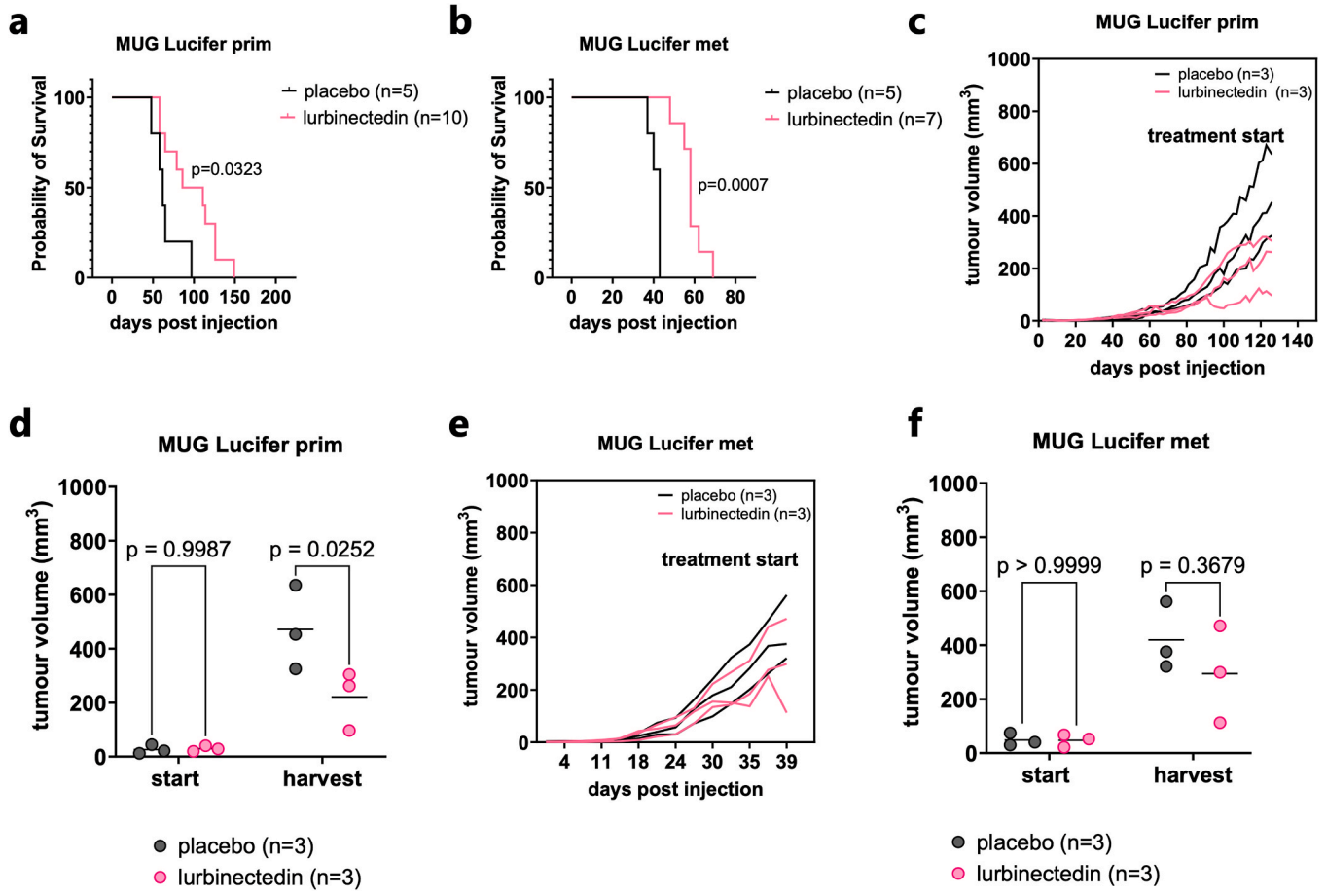

Fig. 3. Differential responses to lurbinectedin in primary and metastatic CCS xenografts
(**a**) Schematic overview of the in vivo experiments. Overview was created with BioRender.com (**b**) Survival curves for MUG Lucifer prim xenografts treated either with three doses of 0.18 mg kg^{-1} lurbinectedin (n = 10) or the equal amount of placebo (n = 5). Mice were sacrificed when tumour volume reached at least 1000 mm^3 or when animals met humane endpoint criteria (≥20 % body weight loss or overall poor health). Tumour growth was monitored until endpoint, and survival curves were generated accordingly. P-values were calculated using the log-rank (Mantel–Cox) test as implemented in GraphPad Prism. (**c**) Survival curves for MUG Lucifer met xenografts treated either with three doses of 0.18 mg kg^{-1} lurbinectedin (n = 7) or the equal amount of placebo (n = 5) analogous to (b). (**d**) Tumour growth over time for MUG Lucifer prim xenografts of the second experiment (n = 3 per condition). Treatment start is indicated by the dotted line. (**e**) Tumour growth over time for MUG Lucifer met xenografts of the second experiment (n = 3 per condition). Treatment start is indicated by the dotted line. (**f-g**) Tumour volumes at treatment initiation and at harvest for MUG Lucifer prim and MUG Lucifer met xenografts. Statistical analysis was performed using two-way repeated-measures ANOVA, with p-values <0.05 considered significant.

for initial tumor size (average size), and all treatments were started on the same day to exclude any bias (Fig. S3E–H). Under these conditions, we again observed a significant reduction in tumor growth in the MUG Lucifer prim model (Fig. 3c and d). In contrast, in the MUG Lucifer met model, tumor growth was on average lower but did not reach statistical significance, although average tumour sizes were ~30 % lower (Fig. 3e and f).

We also evaluated post-treatment tumour necrosis, which is usually associated with better therapy-response, of all tumour bearing mice from the first experiment previously defined by H&E staining of fixed tumour samples and subsequent histopathological examination (Fig. S3C). MUG Lucifer prim tumours showed a generally higher post-treatment necrosis compared to MUG Lucifer met, which had overall low necrosis in all animals tested (Fig. S3D). However, we did not observe complete post-treatment necrosis (100 %) in any of the samples.

Of note, in the case of a single mouse harboring MUG Lucifer prim (Animal Number "5521–0168"), we observed complete tumour shrinkage. The tumour volume had been steadily increasing following three doses of lurbinectedin, peaking at approximately 200 mm^3, before gradually diminishing two months after the final dose administration (Fig. S4A and C). H&E staining of the excised tumour confirmed also the absence of residual tumour cells in the specimen (Fig. S4B). However, this phenomenon was only observed in one mouse, thus limiting significance of the finding.

To control for side effects, as lurbinectedin induced cytotoxic effects at higher concentrations in vitro, we examined mice regarding their state of health over the course of the treatment, including assessment of body weight, blood levels, and organ toxicity. Body weight of the mice did not significantly change in any mouse, confirming that lurbinectedin did not induce any cachectic effects (Fig. S5G–H). Also, no morphological abnormalities could be detected in organs (lung, liver, spleen and kidney in neither control nor treatment groups (Fig. S5I). On the other hand, while red blood cells and platelets remained the same in both groups (treated vs. vehicle, we did observe a significant decrease of lymphocytes and increase of granulocytes in lurbinectedin treated MUG Lucifer prim, changing the distribution of white blood cells (lymphocytes (LYMPH), granulocytes (GRAN) and monocytes (MON)) (Fig. S5A–F). In particular, significant inflammation of tail veins was observed for some mice, which was the main reason for premature termination of the experiment (Fig. S5J). We counteracted by iodine spray treatment which ablated this problem for the other animals.

3.4. Lurbinectedin induces cell line specific modulation of the p53 pathway

As MUG Lucifer prim and MUG Lucifer met demonstrated both in vitro as well as in vivo a different behavior and response to lurbinectedin exposure, besides being derived from the same patient, we postulated that their drug sensitivities and response could be related to differences in transcriptional signatures. To identify key features, we performed RNA sequencing (RNA-Seq) of both cell lines prior and post treatment with lurbinectedin to achieve insight on metastasis driven differences as well as treatment induced changes in gene expression. Indeed, we already observed an enormous set of differentially expressed genes (DEG) in MUG Lucifer met compared to MUG Lucifer prim creating a distinct transcriptional profile for the metastatic lesion (Fig. 4a). Pathway analysis of DEGs using KEGG pathway database revealed these genes to be enriched in cell adhesion molecules, focal adhesion and the

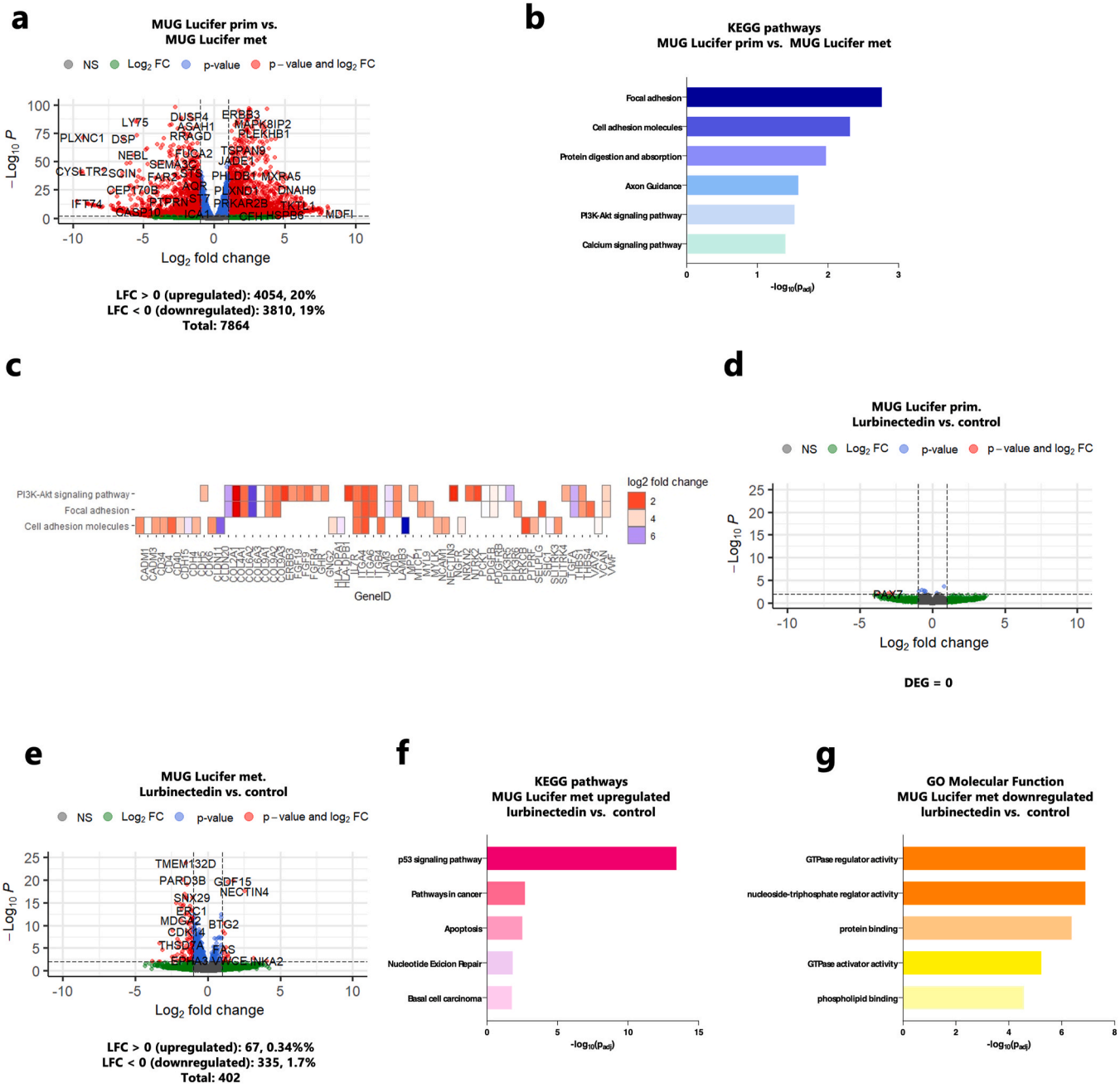

Fig. 4. Primary and metastatic CCS exhibit distinct transcriptional profiles prior and post treatment with lurbinectedin
(**a**) Volcano plots of differentially expressed genes in MUG Lucifer met compared to MUG Lucifer prim (n = 3 for each condition). Genes that did not pass the adjusted p-value threshold and log2 fold-change threshold (not significant) are shown in grey, genes passing the log2 fold-change threshold in green, genes passing the adjusted p-value threshold in blue and genes passing both the adjusted p-value threshold and the log2 fold-change threshold in red. (**b**) KEGG-Pathways of DEG LF2C > 3.5 and LF2C < −3.5, $p_{adj} < 0.05$ enriched in MUG Lucifer met compared to MUG Lucifer prim (**c**) Volcano plots of differentially expressed genes in MUG Lucifer prim after exposure to lurbinectedin for 6h (n = 3 for each condition). (**d**) Volcano plots of differentially expressed genes in MUG Lucifer met after exposure to lurbinectedin for 6h (n = 3 for each condition). **(e)** KEGG-Pathways of upregulated genes $p_{adj} < 0.05$, LF2C > 0 enriched in lurbinectedin treated MUG Lucifer met. **(f)** GO Molecular Function terms enriched in downregulated genes $p_{adj} < 0.05$, LF2C < 0 enriched in lurbinectedin treated MUG Lucifer met. (For interpretation of the references to colour in this figure legend, the reader is referred to the Web version of this article.)

PI3K-Akt pathway, providing evidence of a "metastatic switch" in the MUG Lucifer model (Fig. 4b). Sequencing of matched primary and metastatic clear cell sarcoma revealed enrichment in focal adhesion, cell adhesion molecules, and PI3K/AKT signaling, with several genes from our dataset supporting these pathways. Among these were ECM remodeling factors such as *COL6A3*, *COL2A1*, and *THBS1*, adhesion molecules including *CLDN20*, *MPZ*, and integrins (*ITGA4*, *ITGA6*), as well as PI3K/AKT components like *PIK3R5/6*, *ERBB3*, and *FGF9/19*, all pointing to reinforced cell–matrix interactions and pro-survival signaling in the metastatic setting (Fig. 4c).

Next, we analyzed gene expression changes in MUG Lucifer prim and MUG Lucifer met upon lurbinectedin exposure. To limit

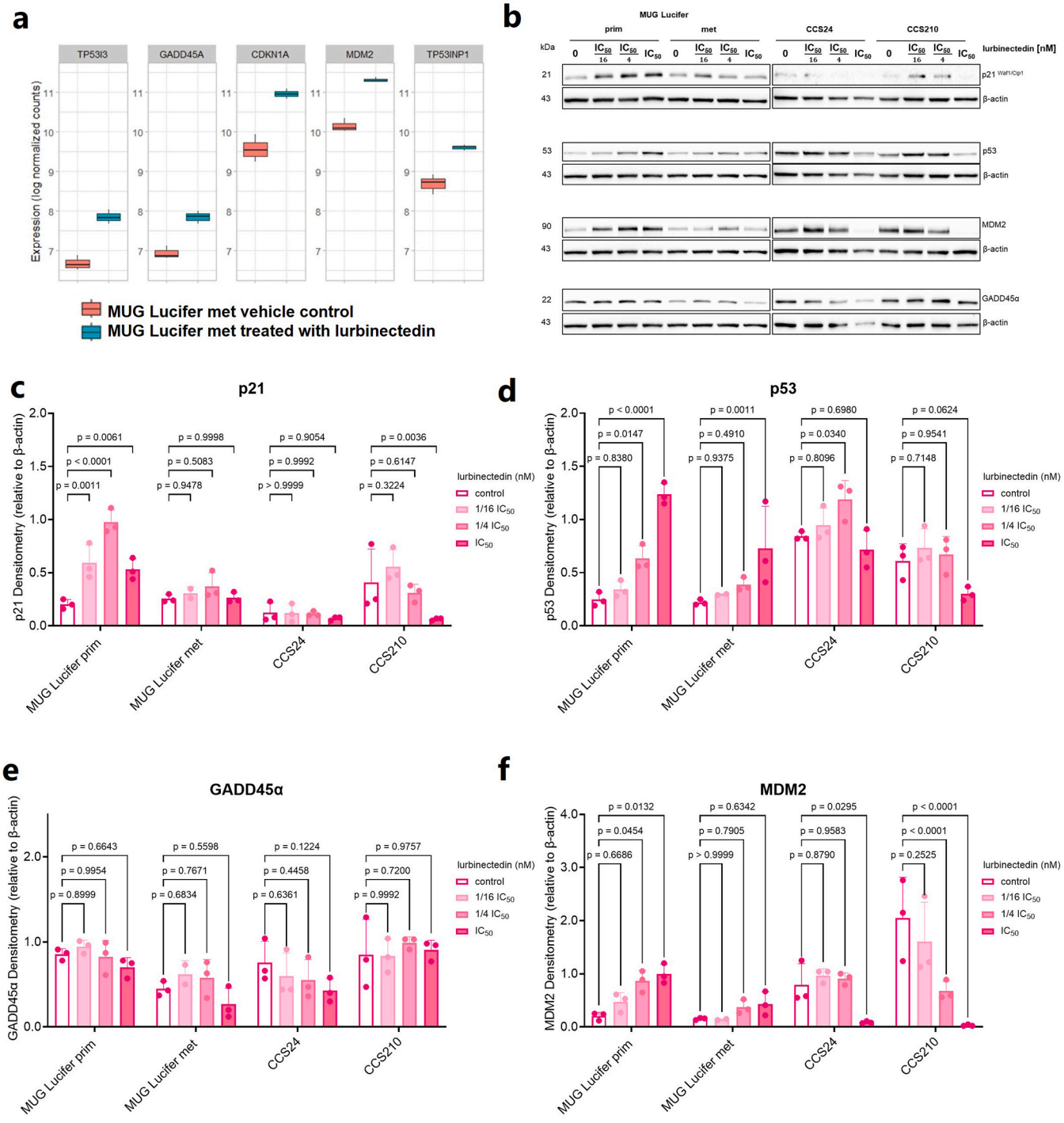

Fig. 5. Lurbinectedin induces p53 activation in MUG Lucifer prim

(**a**) Box plot showing gene expression from RNA sequencing results for selected upregulated genes in MUG Lucifer met after lurbinectedin treatment. (**b**) Protein expression of $p21^{Waf1/Cip1}$, p53, MDM2 and GADD45A were analyzed by immunoblotting under control conditions versus after treatment for cell lines MUG Lucifer prim, MUG Lucifer met, CCS24 and CCS210. Chosen concentrations correspond to the IC_{50} of each cell line (highest concentration) and two subsequent fourfold serial dilutions ($IC_{50}/4$, $IC_{50}/16$). Summary table for IC_{50} values is provided in the supplements. β-actin was used as loading control. Full-length blots for each replicate are presented in supplementary material. (**c-f**) Densitometry quantification of immunoblotting results for each protein. Samples were normalized to loading controls (mean ± SD of $n = 3$). Statistical analysis was performed using Two-way ANOVA with p-values <0.05 were considered significant.

overrepresentation of apoptotic genes, we treated cells for 6h with the respective IC_{50} values for each cell line. Unexpectedly, after 6h on lurbinectedin, gene expression was only altered in MUG Lucifer met, with a total of 402 being dysregulated, whereas no differentially expressed genes could be detected for MUG Lucifer prim despite being treated under the same conditions in both cases (Fig. 4d). Out of 402 genes dysregulated genes in MUG Lucifer met, 67 were upregulated and 335 were downregulated upon treatment with $p_{adj} < 0.05$ indicating a strong inhibition of transcription already after 6h (Fig. 4e). Downstream pathway analysis of upregulated genes highlighted the activation of the p53 pathway, apoptosis and nucleotide excision repair, all related to DNA damage response (Fig. 4f). Furthermore, analyzing downregulated genes in a similar manner using gene onotology (GO) molecular function terms, revealed the impairment of GTPase activity. (Fig. 4g). In the p53 pathway, several key genes were significantly upregulated, including Cyclin-Dependent Kinase Inhibitor 1A (CDKN1A), Mouse Double Minute 2 Homolog (MDM2), Growth Arrest and DNA Damage-Inducible Protein 45 (GADD45), and two genes that are directly induced by p53, namely TP53-Induced Protein Nuclear (TP53INP1) and TP53-Induced Protein 3 (TP53I3) (Fig. 5a). All genes play a role in p53 mediated cell death and response to cellular stress. Based on this, we decided to validate our RNA-Seq results at the protein level by conducting immunoblotting experiments on selected upregulated genes from the p53 pathway, including MDM2, CDKN1A (p21), GADD45, and p53 (Fig. 5b). We treated both MUG Lucifer prim and MUG Lucifer met with increasing concentrations of lurbinectedin and performed western blotting analysis with antibodies against p53, p21, MDM2 and GADD45. Surprisingly, for MUG Lucifer prim, we observed a dose-dependent expression of MDM2, p21, and p53, whereas for MUG Lucifer met, neither showed increased expression, providing evidence for an impaired p53 pathway despite being upregulated in the RNA-Seq data (Fig. 5c–e). For GADD45α we observed no significant differences in neither cell line upon treatment (Fig. 5f). Next, we examined whether the inactivation of p53 in MUG Lucifer met is due to a mutation that could impair p53-mediated apoptosis, using Next-Generation Sequencing of the TP53 amplicon panel. No mutations were found in either cell line, providing evidence that the inactivation of p53 is due to functional impairment rather than a genetic mutation. We next assessed whether similar patterns could be observed in the two additional cell lines from the initial drug screen, CCS24 and CCS210 (Fig. 5b–f). The phenotypic origin of these cell lines is not known, however, we still sought to examine whether the p53 response patterns observed in the MUG Lucifer models were similar in other patient-derived cell lines. Interestingly, CCS24 displayed an increase in p53 without induction of p21 or MDM2, and no caspase activation was detected (Fig. 5b–f, Fig. S6A). By contrast, CCS210 showed no stabilization of p53 and even downregulation of p21 and MDM2, yet exhibited clear caspase activation, consistent with a p53-independent apoptotic mechanism (Fig. 5b–f, Fig. S6A). Together, these findings indicate that while MUG Lucifer prim undergoes canonical p53 activation and apoptosis upon lurbinectedin treatment, MUG Lucifer met and CCS24 display impaired or abortive p53 signaling, and CCS210 engages apoptosis through a p53-independent pathway (Table 2).

Based on these observations, we hypothesized that Akt signaling might contribute to impaired p53 activity, consistent with the upregulation of PI3K-associated genes in our transcriptomic data. To explore this, we assessed the phosphorylation status of Akt in all four cell lines following lurbinectedin treatment (Fig. S6B). While the differences were not statistically significant, the two cell lines without caspase activation, MUG Lucifer met and CCS24 showed higher levels of activated Akt (pAkt/total Akt ratios) compared with the other two lines (Fig. S6C–D). To further examine whether enhanced Akt signaling is directly linked to the p53 defect, we tested functional impairment of the PI3K pathway to assess its role in blocking apoptosis in CCS. However, pharmacological inhibition of pathway components did not restore apoptosis in our experimental system.(Fig. S6F–H).

Table 2
Summarized results for experiments determining mode of cell death.

Marker	MUG Lucifer prim	MUG Lucifer met	CCS24	CCS210
p21	↑	≈	≈	↓
p53	↑	↑	↓	≈
MDM2	↑	≈	≈	↓
Caspase 3/7	yes	no	no	yes
Proposed mode of cell death	**Classical, p53 dependent apoptosis**	**non apoptotic, defective downstream signalling**	**Partial apoptotic response, transient activation of p53**	**P53 independent apoptosis**

Arrows indicate concentration-dependent increase (↑) or decrease (↓) of expression in immunoblotting experiments of CCS cell lines upon treatment with lurbinectedin, whereas ≈ indicates no significant differences.

3.5. Cancer-associated fibroblasts affect drug efficacy of lurbinectedin

The tumour microenvironment is a key driver of drug resistance, with stromal and immune components playing critical roles in modulating therapeutic responses. In conventional in vitro settings, tumour cells are typically studied in isolation, both in vitro and in vivo, which overlooks the contribution of surrounding non-malignant cells [34]. To address this limitation, we investigated whether stromal components influence drug efficacy by establishing a co-culture system with patient-matched cancer-associated fibroblasts, creating a more complex autologous 3D spheroid model of MUG Lucifer prim and met. We isolated CAF cells from tumour surrounding tissue of the same tissue MUG Lucifer prim was derived. We then established a continuous cell line through subsequent immortalization by lentiviral transduction of the hTERT gene analogously to our hTERT NHDF cell line, which was used as a normal control in previous experiments [17]. The new MUG Lucifer hTERT CAF cell line was comprehensibly characterized according to recommendations stated in a consensus statement about working with CAF and compared to the MUG Lucifer hTERT NHDF cell line [35]. Briefly, we first checked for expression of α-smooth muscle actin (α-SMA, ACTA2), and tenascin C (TNC) which are reported CAF markers. Indeed, immunohistochemistry staining revealed that MUG Lucifer hTERT CAF stained positively for α-SMA expression, whereas no positive cells could be detected for MUG Lucifer hTERT NHDF, whereas both were positive for TNC (Fig. 6a). Besides the expression of α-SMA, MUG Lucifer CAF also differ to MUG Lucifer NHDF in terms of morphology and copy number variation profiles (Fig. 6a, Fig. S7B). In addition, we confirmed the absence of tumour cells by the lack of characteristic CCS markers including SOX-10, Melan-A, HMB45 and the gene-fusion *EWSR::ATF1* in both cell lines (Fig. S7A, Table S2). A detailed summary and direct comparison to the NHDF cell line is summarized in Table S3.

Due to the non-uniform distribution of stroma around tumour cells in sarcoma, we experimented with varying ratios of CAF to evaluate their impact on drug response. Co-cultivation of tumour cells with CAFs resulted in the formation of denser, more compact spheroids compared to tumour cells cultivated alone, particularly noticeable with higher ratios of fibroblasts (Fig. 6b). To simplify, cultivation of MUG Lucifer hTERT CAF with MUG Lucifer prim was titled Co-Culture (prim), whereas the co-cultivation with MUG Lucifer met is referred to as Co-Culture (met). MUG Lucifer prim cells preferentially accumulated in the core of the spheroid surrounded by fibroblasts, resembling the original tumour tissue, but also occurred all over the spheroid as observed for MUG Lucifer met (Fig. 6c). Interestingly, when cocultured with tumor cells, CAFs exhibited a marked increase in α-SMA expression compared to the monoculture, with virtually all CAFs within the spheroids staining positive. In contrast, NHDFs remained negative for α-SMA both in mono- and coculture conditions indicating that tumor-

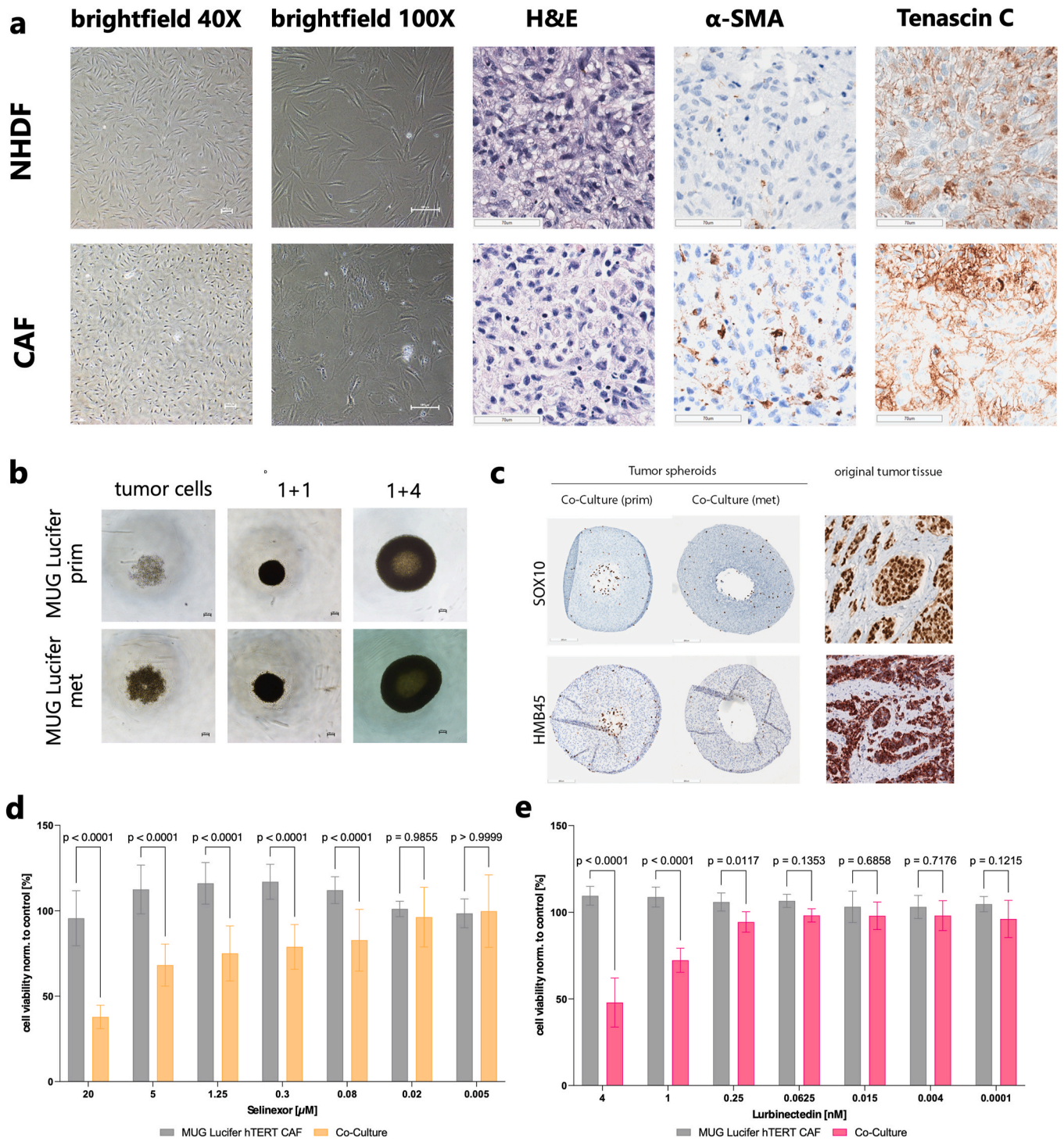

Fig. 6. Establishment of a new MUG Lucifer co-culture model

(**a**) Characterization of MUG Lucifer hTERT CAF (cancer-associated fibroblast) in comparison with MUG Lucifer hTERT NHDF (normal human dermal fibroblast). Both fibroblast populations were derived from the same patient from whom the MUG Lucifer tumor cell lines originated. Monolayer morphology of MUG Lucifer hTERT NHDF showed more elongated, spindle-shaped cells compared with MUG Lucifer hTERT CAF (brightfield and H&E staining). Cell lines were stained for fibroblast markers α-SMA and tenascin C to confirm differential expression between CAF and NHDF. (**b**) Spheroid formation of MUG Lucifer prim and MUG Lucifer met cultivated with different ratios of MUG Lucifer hTERT CAF. Scale bar depicted are 100 μm. (**c**) Immunohistochemistry of multicellular spheroids (1 + 4 ratio) compared to the original tumour tissue. Scale bars depicted are 200 μm. (**d**) Dose response for selinexor treatment in MUG Lucifer hTERT CAF spheroids and its Co-Culture with MUG Lucifer prim. (**e**) Dose response for lurbinectedin treatment in MUG Lucifer hTERT CAF spheroids and its Co-Culture with MUG Lucifer prim.

derived cues strongly enhance the myofibroblastic phenotype of CAFs, whereas normal fibroblasts remain unresponsive (Fig. S7C). Using our new model we first checked whether single-agents were able to reduce the cell viability of multicellular spheroids and observed that an almost five fold higher concentration was needed to achieve the same effect as with the tumour cells alone in both cases (Fig. 6d and e). Of note, MUG Lucifer hTERT CAF alone were not affected by the same concentrations used for the multicellular spheroids (Fig. 6d and e).

3.6. Lurbinectedin synergizes with selinexor in vitro

Although lurbinectedin as a single agent prolonged survival in both MUG Lucifer xenografts, its effect on MUG Lucifer met xenografts remained moderate due to their aggressive behavior in vivo. This moderate response could only be partially explained by differences in their transcriptomic profiles. Moreover, given that single-agent therapies are generally unlikely to produce significant clinical benefit for cancer patients, we aimed to optimize the treatment strategy by exploring combinational approaches. To identify promising combinations, we pursued two strategies (i) selecting additional top candidates from the initial drug screen and (ii) simultaneously targeting both tumor cells and cancer-associated fibroblasts (CAFs).

To further investigate the role of stromal components in drug response, we performed a secondary drug screen using a subset of compounds with slight variations from the initial screen. In this experiment, drugs were tested on MUG Lucifer hTERT CAF and the corresponding MUG Lucifer hTERT NHDF with the aim of identifying potential CAF-specific vulnerabilities. Although most of the tested agents are not primarily designed to target fibroblasts, we observed notable differences between CAFs and NHDFs. Overall, both fibroblast populations displayed higher AUC values compared to tumor cells; however, several compounds demonstrated relatively greater activity in CAFs. The top hits were primarily proteasome inhibitors, tyrosine kinase inhibitors, and FGFR inhibitors, along with selinexor and panobinostat, which had also emerged as leading candidates in the initial drug screening of the tumor cells (Fig. 7a, Table S3). Both selinexor and panobinostat, exhibited better efficacy towards metastatic CCS in the drug screening, however selinexor demonstrated less cytotoxicity towards normal fibroblasts of the MUG Lucifer patient enabling potential lowering of lurbinectedin concentrations for less side effects and targeting metastasis. In single cell cultures using both MUG Lucifer cell lines, combinational treatment was carried out in a similar setup to the drug screening, using serial dilutions based on the IC_{50} values determined in the drug screening of both compounds in a 6x6 matrix format ensuring all possible combinations. Relative synergy calculating using a variety of algorithms (Bliss, ZIP, HSA and Loewe) is portrayed as a 3D heatmap of each dose in the CCS cell lines MUG Lucifer prim and MUG

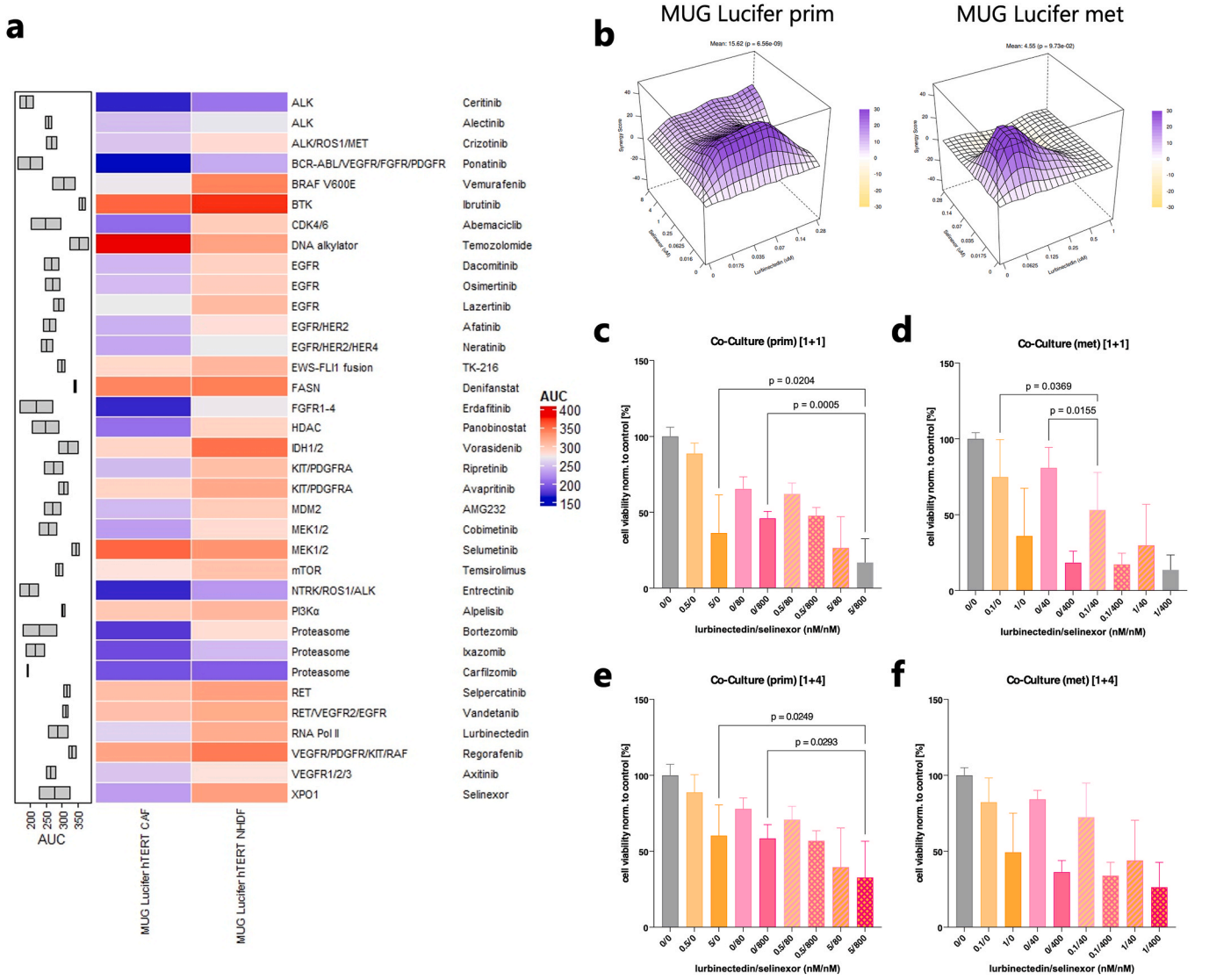

Fig. 7. Combinational treatment of lurbinectedin and selinexor
(**a**) Heat map portraying AUC values for compounds tested on MUG Lucifer fibroblast cell lines from the same patient sorted by target group. (**b**) Synergy scores of combinational treatment for MUG Lucifer prim and MUG Lucifer met single cultures calculated using the Bliss Algorithm. (**c-d**) Combinational treatment of selinexor and lurbinectedin in Co-Culture (prim) and Co-Culture (met) with equal amount of fibroblasts (**e-f**) Combinational treatment of selinexor and lurbinectedin in Co-culture (prim) and Co-culture (met) with four times more fibroblasts than tumour cells.

Lucifer met (Fig. 7b, Fig. S8A–F). Synergy values for each combination are represented numerically and visually with red and higher positive values indicating increased levels of synergy. Strong synergy (synergy score >10) was observed for most combinations in both cell lines.

We then carried out combinational treatment in the multicellular spheroids with varying ratios of MUG Lucifer hTERT CAF using higher the IC_{50} values determined for single cell spheroids and a 10 fold higher concentration to validate the results. We observed moderate synergy between selinexor and lurbinectedin with significant combinations highlighted, however, it was not as remarkable as observed as for the tumour cells alone, with no significant differences between the two cell lines (Fig. 7c–f and fig. S(G-J).

4. Discussion

Ultra-rare sarcomas such as clear cell sarcoma (CCS) pose major challenges, particularly when they reach metastatic or advanced stages. Their rarity and resistance to conventional chemotherapy severely limit research for novel therapeutic options highlighting the urgent need for innovative approaches. In our previous study, we observed epigenetic differences between primary and metastatic CCS including unique patterns in DNA and Arginine methylation for each phenotype and provided a new therapeutic strategy for tailored therapy using small molecule inhibitors of the Protein Arginine Methyltransferase (PRMT) [17]. Although these inhibitors are emerging as promising candidates in the future for advanced stage solid tumours and have been tested in a recent Phase I clinical trial, they are still far from being used in a clinical setting, especially as a single-agent drug [36].

Here, in our new study, we report a functional drug screen for CCS by repurposing chemotherapeutics and targeted drugs for a faster translation into a clinical setting. Several candidates from this screening showed in vitro efficacy towards all cell lines tested with lurbinectedin portraying the best candidate overall. Owing to the relevance of the results gathered from the clinical trial published elsewhere, lurbinectedin has been approved in several countries for the treatment of patients with metastatic small-cell lung cancer (SCLC) with disease progression on or after platinum-based chemotherapy [37]. Moreover, recent clinical trials have highlighted the potential of lurbinectedin both as a monotherapy and in combination with other agents in SCLC and a range of other tumour entities [38–40]. This trabectedin derivative selectively inhibits oncogenic transcription by hindering RNA polymerase II, affecting DNA repair mechanisms leading to apoptosis in both tumour and tumour-associated stromal cells [41–43].

Preclinical studies have demonstrated the potent anticancer activity of ecteinascidins, such as lurbinectedin and trabectedin, particularly in transcriptionally driven tumours, as they suppress super-enhancer-driven transcription, but also in various other tumour types, underscoring their therapeutic potential beyond currently approved indications [30,44–46].

Even though we are the first to report lurbinectedin efficacy in our patient-derived sarcoma cell lines, this is in line with previous preclinical studies on other sarcoma driven by gene fusions similar to the one occurring in CCS such as desmoplastic round cell tumours and Ewing sarcomas [47,48]. Also, in a recently published phase II trial, 28 pretreated patients with relapsed Ewing sarcoma were administered lurbinectedin, showing a 14.3 % overall response rate and a median response duration of 4.2 months [49]. Furthermore, in a phase II study, Cote et al. reported evidence of clinical benefit of lurbinectedin in combination with doxorubicin in other fusion driven sarcoma, including synovial sarcoma and myxoid liposarcoma, but also in non-fusion driven sarcoma subtypes, such as leiomyosarcomas and dedifferentiated liposarcomas [50]. Clinical benefits were observed in 39.3 % of patients, with disease control in 57.1 %. The safety profile was manageable, though severe hematologic abnormalities were more frequent due to heavy pretreatment. The study recommends primary G-CSF (granulocyte colony-stimulating factor) prophylaxis for patients on lurbinectedin. The results suggest that lurbinectedin could be a valuable addition to existing therapies for relapsed Ewing sarcoma, addressing a significant unmet medical need. However, it is important to mention that while lurbinectedin shows high efficacy in vitro at low concentrations, the discrepancy between preclinical efficacy and clinical results remains a major challenge. While no clinical trials have evaluated lurbinectedin specifically in CCS, data on the related compound trabectedin illustrate this limitation, with progressive disease reported in two CCS patients [51], one stable and one progressive case [52] and a single partial response [53]. These findings and the narrow therapeutic window, suggest that similar translational challenges could apply to lurbinectedin. Therefore, while individual patients may benefit, the translation of preclinical findings into significant clinical activity has been only moderately successful to date and requires further investigation.

Our findings suggest that lurbinectedin triggers distinct, context-dependent cell death mechanisms in CCS. In MUG Lucifer prim cells, it activated p53 signaling and apoptosis, while the metastatic MUG Lucifer met cells showed transcriptomic changes without corresponding protein-level activation. Additional cell lines, CCS24 and CCS210, revealed yet other forms of cell death, underscoring that lurbinectedin-induced responses are shaped by inter-tumour heterogeneity. These discrepancies may stem from post-transcriptional regulation, tumour evolution, or alternative survival pathways as the PI3K-Akt pathway, which is enriched in our RNA Seq data of the metastatic cell line and reported to have multiple roles in preventing apoptosis in cancer, as well as promoting metastasis [54–56]. Importantly, the type of cell death, apoptosis versus necrosis or other pathways, has major implications for treatment outcome, as controlled forms like apoptosis limit inflammation, whereas uncontrolled forms may promote tumour progression and immune evasion [57,58]. Assessing these mechanisms is therefore critical for understanding resistance and refining therapeutic strategies with lurbinectedin. Chemotherapeutic agents that are usually used for soft tissue sarcoma demonstrated limited efficacy in metastatic CCS [8]. Additionally, also targeted therapies including pazopanib, sunitinib and crizotinib have a limited activity in these tumours, which our used model is as well resistant to Refs. [8,59]. Hence, any improvement of survival is considered a valuable progress.

Further undermining the importance of modeling metastatic disease and representing cellular plasticity in preclinical studies, is the significant differences in gene expression between matched primary and metastatic cell lines of the same CCS patient, we noted in our study. Numerous studies on other cancer entities suggest that metastases can differ from their matched primary tumour in many aspects, despite sharing similar dominant genomic patterns, including epigenetic and transcriptional profiles [60–64]. Consequently, considering the plasticity tailoring to metastatic cells should be considered when designing treatment strategies [12,65]. This is especially true for sarcoma, considering they are not epithelial cells, and thus cannot undergo the conventional epithelial to mesenchymal transition responsible for metastasis in other cancers.

We cannot exclude that some of these differences are due to anatomical localization of the tumour or treatment regime of the patient prior to isolation, as we only have one matched pair due to the low incidence of the disease. The enormous gene set affected still provides evidence of a unique transcriptional signature of metastatic CCS and can therefore serve as a potential platform for identifying metastasis in CCS earlier on. Whether these characteristics can be exploited as a biomarker requires further investigation beyond the scope of this article.

Furthermore, in vitro cultures encounter numerous challenges in recapitulating crucial aspects of cancer, such as interactions with stromal cells and the physical components of the tumour microenvironment (TME), within experimental settings [66]. In an attempt to model this in vitro without the involvement of animal experiments, we successfully established the continuous cell line MUG Lucifer hTERT CAF as a new addition to the previous MUG Lucifer cell lines. This new fibroblast cell

line was derived from the tumour microenvironment of the primary tumour, differing from the normal human dermal fibroblast cell line, we established as a non-malignant control in our previous publication. Stromal components of tumours, particularly cancer associated fibroblasts, can significantly alter drug response and play various role in drug resistance due to their resilient behavior [67–69]. Co-culturing the CAF cell line with the tumour cell lines revealed that both the initial efficacy observed in monotherapy and the combinational treatment, when tested on tumour cells alone, were diminished. This effect was only seen at high concentrations of both agents in one of the cell lines, suggesting that the presence of stromal components hampers the drug response. Subcutaneous mouse models typically lack the stromal environment present in patients, as the tumours formed in these models are often encapsulated and less invasive. Therefore, it may be important to assess the distribution of stromal components in sarcoma tumours before designing treatment strategies. Similar observations were reported in a clinical setting, where the sarcoma TME predicted both survival and response to immunotherapy [70]. While this co-culture model enhances the in vitro system and represents a step toward better recapitulating the tumour microenvironment (TME), it still lacks key components, including immune cells and the full stromal composition found in patient tumours. These limitations reduce its applicability for studying immune responses and drug interactions in a more physiologically relevant context. Additionally, single-cell RNA sequencing could provide deeper mechanistic insights into the cellular response to lurbinectedin; however, to yield meaningful results, it would need to be performed on orthotopic models, ex vivo patient explants, or co-cultures with immune cells. These approaches remain challenging and were beyond the scope of this study but should be a key focus for future investigations.

Finally, to our best knowledge, we are the first to report the synergistic effects of lurbinectedin and selinexor, a selective inhibitor of Exportin-1 (XPO1), a nuclear transport protein, which is used in the treatment of diffuse large B-cell lymphoma and multiple myeloma for sarcoma treatment [71,72]. We demonstrated that this combination was highly synergistic in both primary and metastatic CCS in vitro cultures.

In summary, our findings suggest that lurbinectedin may represent a potential therapeutic option for targeting clear cell sarcoma (CCS), although it is important to note that this is a drug screen in a highly resistant, ultra-rare sarcoma subtype. While the drug screen results and testing in spheroids and in vivo models indicate some activity, it is essential to consider the challenges and limitations of treating CCS, a disease known for its resistance to available treatments. Our study also highlights the need for a deeper understanding of cellular plasticity and metastatic features when using preclinical models for therapeutic exploration.

Moreover, this research provides a foundation for further investigation into other potential therapies beyond lurbinectedin, particularly in relation to the transcriptomic features of CCS metastasis and drug sensitivities targeting specific pathways. While our findings contribute to the ongoing efforts to identify therapeutic strategies for CCS, it is clear that more work is needed to improve treatment outcomes in this and other difficult-to-treat cancers. Translating these approaches and insights to other cancer types may also help to uncover new vulnerabilities for targeted therapy.

CRediT authorship contribution statement

Djenana Vejzovic: Writing – original draft, Visualization, Validation, Investigation, Formal analysis, Conceptualization. **Christina Karner:** Validation, Investigation. **Karoline Fechter:** Validation, Investigation. **Gerald Ritter:** Validation, Investigation. **Viktoria Holzer:** Validation, Investigation. **Lisa Barones:** Investigation. **Nina A. Schweintzger:** Visualization, Investigation, Formal analysis, Data curation. **Karin Wagner:** Investigation. **Freya Lyssy:** Visualization, Investigation. **Martin Gauster:** Resources. **Joanna Szkandera:** Resources. **Stefanie Stanzer:** Visualization, Resources, Investigation, Formal analysis. **Barbara Prietl:** Software, Investigation, Formal analysis. **Amin El-Heliebi:** Resources, Investigation, Formal analysis. **Birgit Lohberger:** Resources, Investigation, Formal analysis. **Maria Jose Guillén-Navaro:** Resources. **Pablo M. Avilés:** Resources. **Iva Brčić:** Resources, Investigation. **Bernadette Liegl-Atzwanger:** Resources, Investigation. **Beate Rinner:** Writing – original draft, Supervision, Project administration, Funding acquisition, Conceptualization.

Ethics approval and consent to participate

The study was approved by the ethics committee of the Medical University of Graz (vote 31–457 ex 18/19). Animal work was carefully carried out in accordance with a protocol approved by the institutional animal care and use committee of the Austrian Federal Ministry of Science and Research (BMWFW) (vote 66.010/0046-WF/V/3b/2016 amendment GZ 2023–0.288.358).

Consent for publication

All authors agreed to the publication of this article.

Funding information

This work was partially funded by PharmaMar S.A.

Declaration of competing interest

The authors declare the following financial interests/personal relationships which may be considered as potential competing interests: Beate Rinner reports financial support was provided by PharmaMar SA. Maria J. Guillen-Navarro reports a relationship with PharmaMar SA that includes: employment. Pablo M. Aviles reports a relationship with PharmaMar SA that includes: employment. If there are other authors, they declare that they have no known competing financial interests or personal relationships that could have appeared to influence the work reported in this paper.

Acknowledgments

We sincerely thank Katharina Meditz and Dietmar Glänzer for technical support in cell culture experiments and Zoran Mitrović for help in blood analysis measurements.

Appendix A. Supplementary data

Supplementary data to this article can be found online at https://doi.org/10.1016/j.canlet.2025.218131.

Data availability

All data generated in this study are included in the published article, the supplements of are available from the corresponding author upon request. RNA Sequencing data were deposited at the Sequence Read Archive (SRA) under the BioProjectID PRJNA1160044.

References

[1] L.J. Helman, P. Meltzer, Mechanisms of sarcoma development, Nat. Rev. Cancer 3 (9) (2003) 685–694.
[2] A. Italiano, S. Mathoulin-Pelissier, A.L. Cesne, P. Terrier, S. Bonvalot, F. Collin, et al., Trends in survival for patients with metastatic soft-tissue sarcoma, Cancer 117 (5) (2011) 1049–1054.
[3] B.S. Taylor, J. Barretina, R.G. Maki, C.R. Antonescu, S. Singer, M. Ladanyi, Advances in sarcoma genomics and new therapeutic targets, Nat. Rev. Cancer 11 (8) (2011) 541–557.
[4] J. Zucman, O. Delattre, C. Desmaze, A.L. Epstein, G. Stenman, F. Speleman, et al., EWS and ATF-1 gene fusion induced by t(12;22) translocation in malignant melanoma of soft parts, Nat. Genet. 4 (4) (1993) 341–345.

[5] B.A. Nacev, K.B. Jones, A.M. Intlekofer, J.S.E. Yu, C.D. Allis, W.D. Tap, et al., The epigenomics of sarcoma, Nat. Rev. Cancer 20 (10) (2020) 608–623.
[6] M. Hisaoka, T. Ishida, T.T. Kuo, A. Matsuyama, T. Imamura, K. Nishida, et al., Clear cell sarcoma of soft tissue: a clinicopathologic, immunohistochemical, and molecular analysis of 33 cases, Am. J. Surg. Pathol. 32 (3) (2008) 452–460.
[7] M. Linch, A.B. Miah, K. Thway, I.R. Judson, C. Benson, Systemic treatment of soft-tissue sarcoma-gold standard and novel therapies, Nat. Rev. Clin. Oncol. 11 (4) (2014) 187–202.
[8] A. Smrke, A.M. Frezza, C. Giani, N. Somaiah, M. Brahmi, A.M. Czarnecka, et al., Systemic treatment of advanced clear cell sarcoma: results from a retrospective international series from the World Sarcoma Network, ESMO Open 7 (3) (2022) 100522.
[9] C. Le Tourneau, J.P. Delord, A. Gonçalves, C. Gavoille, C. Dubot, N. Isambert, et al., Molecularly targeted therapy based on tumour molecular profiling versus conventional therapy for advanced cancer (SHIVA): a multicentre, open-label, proof-of-concept, randomised, controlled phase 2 trial, Lancet Oncol. 16 (13) (2015) 1324–1334.
[10] P.J. O'Dwyer, R.J. Gray, K.T. Flaherty, A.P. Chen, S. Li, V. Wang, et al., The NCI-MATCH trial: lessons for precision oncology, Nat. Med. 29 (6) (2023) 1349–1357.
[11] D.B. Johnson, F. Zhao, M. Noel, G.J. Riely, E.P. Mitchell, J.J. Wright, et al., Trametinib activity in patients with solid tumors and Lymphomas harboring BRAF Non-V600 mutations or fusions: results from NCI-MATCH (EAY131), Clin. Cancer Res. 26 (8) (2020) 1812–1819.
[12] K. Ganesh, J. Massagué, Targeting metastatic cancer, Nat. Med. 27 (1) (2021) 34–44.
[13] C. Kornauth, T. Pemovska, G.I. Vladimer, G. Bayer, M. Bergmann, S. Eder, et al., Functional precision medicine provides clinical benefit in advanced aggressive hematologic cancers and identifies exceptional responders, Cancer Discov. 12 (2) (2022) 372–387.
[14] E. Bangi, C. Ang, P. Smibert, A.V. Uzilov, A.G. Teague, Y. Antipin, et al., A personalized platform identifies trametinib plus zoledronate for a patient with KRAS-mutant metastatic colorectal cancer, Sci. Adv. 5 (5) (2019) eaav6528.
[15] T. Ranjan, S. Sengupta, M.J. Glantz, R.M. Green, A. Yu, D. Aregawi, et al., Cancer stem cell assay-guided chemotherapy improves survival of patients with recurrent glioblastoma in a randomized trial, Cell Rep. Med. 4 (5) (2023) 101025.
[16] D. Malani, A. Kumar, O. Brück, M. Kontro, B. Yadav, M. Hellesøy, et al., Implementing a functional precision medicine Tumor Board for Acute Myeloid leukemia, Cancer Discov. 12 (2) (2022) 388–401.
[17] C. Karner, I. Anders, D. Vejzovic, J. Szkandera, S. Scheipl, A.J.A. Deutsch, et al., Targeting epigenetic features in clear cell sarcomas based on patient-derived cell lines, J. Transl. Med. 21 (1) (2023) 54.
[18] J.K. Lee, Z. Liu, J.K. Sa, S. Shin, J. Wang, M. Bordyuh, et al., Pharmacogenomic landscape of patient-derived tumor cells informs precision oncology therapy, Nat. Genet. 50 (10) (2018) 1399–1411.
[19] A. Ianevski, A.K. Giri, T. Aittokallio, SynergyFinder 3.0: an interactive analysis and consensus interpretation of multi-drug synergies across multiple samples, Nucleic Acids Res. 50 (W1) (2022). W739-w43.
[20] P. Ewels, M. Magnusson, S. Lundin, M. Käller, MultiQC: summarize analysis results for multiple tools and samples in a single report, Bioinformatics 32 (19) (2016) 3047–3048.
[21] A. Dobin, C.A. Davis, F. Schlesinger, J. Drenkow, C. Zaleski, S. Jha, et al., STAR: ultrafast universal RNA-seq aligner, Bioinformatics 29 (1) (2013) 15–21.
[22] P. Danecek, J.K. Bonfield, J. Liddle, J. Marshall, V. Ohan, M.O. Pollard, et al., Twelve years of SAMtools and BCFtools, GigaScience 10 (2) (2021).
[23] Y. Liao, G.K. Smyth, W. Shi, featureCounts: an efficient general purpose program for assigning sequence reads to genomic features, Bioinformatics 30 (7) (2014) 923–930.
[24] M.I. Love, W. Huber, S. Anders, Moderated estimation of fold change and dispersion for RNA-seq data with DESeq2, Genome Biol. 15 (12) (2014) 550.
[25] N. Ignatiadis, B. Klaus, J.B. Zaugg, W. Huber, Data-driven hypothesis weighting increases detection power in genome-scale multiple testing, Nat. Methods 13 (7) (2016) 577–580.
[26] Z. Gu, R. Eils, M. Schlesner, Complex heatmaps reveal patterns and correlations in multidimensional genomic data, Bioinformatics 32 (18) (2016) 2847–2849.
[27] N. Percie du Sert, V. Hurst, A. Ahluwalia, S. Alam, M.T. Avey, M. Baker, et al., The ARRIVE guidelines 2.0: updated guidelines for reporting animal research, BMJ Open Sci 4 (1) (2020) e100115.
[28] F. Lyssy, D. Forstner, B.A. Brugger, K. Ujčič, J. Guettler, N. Kupper, et al., The chicken chorioallantoic membrane assay revisited - a face-lifted approach for new perspectives in placenta research, Placenta 166 (2024) 77–84.
[29] K.M. Joo, J. Kim, J. Jin, M. Kim, H.J. Seol, J. Muradov, et al., Patient-specific orthotopic glioblastoma xenograft models recapitulate the histopathology and biology of human glioblastomas in situ, Cell Rep. 3 (1) (2013) 260–273.
[30] M. Cigrang, J. Obid, M. Nogaret, L. Seno, T. Ye, G. Davidson, et al., Pan-inhibition of super-enhancer-driven oncogenic transcription by next-generation synthetic ecteinascidins yields potent anti-cancer activity, Nat. Commun. 16 (1) (2025) 512.
[31] S.Y. Bae, N. Guan, R. Yan, K. Warner, S.D. Taylor, A.S. Meyer, Measurement and models accounting for cell death capture hidden variation in compound response, Cell Death Dis. 11 (4) (2020) 255.
[32] A. Vidal, C. Muñoz, M.J. Guillén, J. Moretó, S. Puertas, M. Martínez-Iniesta, et al., Lurbinectedin (PM01183), a new DNA minor groove binder, inhibits growth of orthotopic primary graft of cisplatin-resistant epithelial ovarian cancer, Clin. Cancer Res. 18 (19) (2012) 5399–5411.
[33] J.F. Leal, M. Martínez-Díez, V. García-Hernández, V. Moneo, A. Domingo, J. A. Bueren-Calabuig, et al., PM01183, a new DNA minor groove covalent binder with potent in vitro and in vivo anti-tumour activity, Br. J. Pharmacol. 161 (5) (2010) 1099–1110.
[34] H. Masuda, Cancer-associated fibroblasts in cancer drug resistance and cancer progression: a review, Cell Death Discov. 11 (1) (2025) 341.
[35] E. Sahai, I. Astsaturov, E. Cukierman, D.G. DeNardo, M. Egeblad, R.M. Evans, et al., A framework for advancing our understanding of cancer-associated fibroblasts, Nat. Rev. Cancer 20 (3) (2020) 174–186.
[36] A.B. El-Khoueiry, J. Clarke, T. Neff, T. Crossman, N. Ratia, C. Rathi, et al., Phase 1 study of GSK3368715, a type I PRMT inhibitor, in patients with advanced solid tumors, Br. J. Cancer 129 (2) (2023) 309–317.
[37] J. Trigo, V. Subbiah, B. Besse, V. Moreno, R. López, M.A. Sala, et al., Lurbinectedin as second-line treatment for patients with small-cell lung cancer: a single-arm, open-label, phase 2 basket trial, Lancet Oncol. 21 (5) (2020) 645–654.
[38] L. Paz-Ares, H. Borghaei, S.V. Liu, S. Peters, R.S. Herbst, K. Stencel, et al., Efficacy and safety of first-line maintenance therapy with lurbinectedin plus atezolizumab in extensive-stage small-cell lung cancer (IMforte): a randomised, multicentre, open-label, phase 3 trial, Lancet 405 (10495) (2025) 2129–2143.
[39] G.M. Cote, S.P. Chawla, G. Demetri, B. Kasper, R.L. Jones, J.M. Broto, et al., SaLudo: a randomized phase IIb/III study of lurbinectedin plus doxorubicin as first-line treatment in leiomyosarcoma, Future Oncol. 21 (8) (2025) 943–951.
[40] A. Falcón, S. Ponce, G.M. Cote, A. Gil, J.J. Lin, B. Bockorny, et al., Phase I results on the efficacy, safety and pharmacokinetics of lurbinectedin and irinotecan in advanced solid tumors, Invest. N. Drugs 43 (4) (2025) 955–967.
[41] C.L. Christensen, N. Kwiatkowski, B.J. Abraham, J. Carretero, F. Al-Shahrour, T. Zhang, et al., Targeting transcriptional addictions in small cell lung cancer with a covalent CDK7 inhibitor, Cancer Cell 26 (6) (2014) 909–922.
[42] Nuñez G. Santamaría, C.M. Robles, C. Giraudon, J.F. Martínez-Leal, E. Compe, F. Coin, et al., Lurbinectedin specifically triggers the degradation of phosphorylated RNA polymerase II and the Formation of DNA breaks in cancer cells, Mol. Cancer Therapeut. 15 (10) (2016) 2399–2412.
[43] C. Belgiovine, E. Bello, M. Liguori, I. Craparotta, L. Mannarino, L. Paracchini, et al., Lurbinectedin reduces tumour-associated macrophages and the inflammatory tumour microenvironment in preclinical models, Br. J. Cancer 117 (5) (2017) 628–638.
[44] E. Gäbele, I. Gigante, M. Pastore, A. Cigliano, G. Galleri, T. Bauer, et al., The DNA minor groove binders trabectedin and lurbinectedin are potent antitumor agents in human intrahepatic cholangiocarcinoma, Int. J. Mol. Sci. 26 (18) (2025).
[45] A. Srivastava, C. Unterweger, S. Guttmann, A. Wolf, L. Müllauer, M. Schepelmann, et al., Therapeutic effects of lurbinectedin in PARP inhibitor-resistant high-grade serous ovarian cancer using patient-derived cell lines and organoid models, Int. J. Mol. Sci. 26 (18) (2025).
[46] A. Laroche-Clary, V. Chaire, V. Valverde, M.A. Derieppe, A. Italiano, Synergistic effects of ATR inhibition and lurbinectedin in soft-tissue sarcomas: the predictive role of SLFN11 expression, Clin. Cancer Res. 31 (17) (2025) 3796–3804.
[47] M.L. Harlow, N. Maloney, J. Roland, M.J. Guillen Navarro, M.K. Easton, S. M. Kitchen-Goosen, et al., Lurbinectedin inactivates the ewing Sarcoma Oncoprotein EWS-FLI1 by redistributing it within the nucleus, Cancer Res. 76 (22) (2016) 6657–6668.
[48] J.M. Gedminas, R. Kaufman, E.A. Boguslawski, A.C. Gross, M. Adams, I. Beddows, et al., Lurbinectedin inhibits the EWS-WT1 transcription factor in desmoplastic small round cell tumor, Mol. Cancer Therapeut. 21 (8) (2022) 1296–1305.
[49] V. Subbiah, I. Braña, A. Longhi, V. Boni, J.P. Delord, A. Awada, et al., Antitumor activity of lurbinectedin, a selective inhibitor of oncogene transcription, in patients with relapsed ewing sarcoma: results of a basket phase II Study, Clin. Cancer Res. 28 (13) (2022) 2762–2770.
[50] G.M. Cote, E. Choy, T. Chen, A. Marino-Enriquez, J. Morgan, P. Merriam, et al., A phase II multi-strata study of lurbinectedin as a single agent or in combination with conventional chemotherapy in metastatic and/or unresectable sarcomas, Eur. J. Cancer 126 (2020) 21–32.
[51] E. Palmerini, R. Sanfilippo, G. Grignani, A. Buonadonna, A. Romanini, G. Badalamenti, et al., Transcription regulators and ultra-rare and other rare translocation-related sarcomas treated with trabectedin: a proof of principle from a post-hoc analysis, Front. Oncol. 12 (2022) 1042479.
[52] A. Le Cesne, S. Cresta, R.G. Maki, J.Y. Blay, J. Verweij, A. Poveda, et al., A retrospective analysis of antitumour activity with trabectedin in translocation-related sarcomas, Eur. J. Cancer 48 (16) (2012) 3036–3044.
[53] M. Galera, R. Álvarez, M. Arregui, M. Paniagua, A. Álvarez, R.A. González Crisostomo, et al., A clear cell sarcoma case: a diagnostic and treatment challenge, with a promising response to trabectedin, Case Rep. Oncol. 16 (1) (2023) 1542–1550.
[54] L.M. Thorpe, H. Yuzugullu, J.J. Zhao, PI3K in cancer: divergent roles of isoforms, modes of activation and therapeutic targeting, Nat. Rev. Cancer 15 (1) (2015) 7–24.
[55] B. Bilanges, Y. Posor, B. Vanhaesebroeck, PI3K isoforms in cell signalling and vesicle trafficking, Nat. Rev. Mol. Cell Biol. 20 (9) (2019) 515–534.
[56] A.E. Shin, K. Sugiura, S.W. Kariuki, D.A. Cohen, S.P. Flashner, A.J. Klein-Szanto, et al., LIN28B-mediated PI3K/AKT pathway activation promotes metastasis in colorectal cancer models, J. Clin. Investig. 135 (8) (2025).
[57] S. Bedoui, M.J. Herold, A. Strasser, Emerging connectivity of programmed cell death pathways and its physiological implications, Nat. Rev. Mol. Cell Biol. 21 (11) (2020) 678–695.
[58] P. Meier, A.J. Legrand, D. Adam, J. Silke, Immunogenic cell death in cancer: targeting necroptosis to induce antitumour immunity, Nat. Rev. Cancer 24 (5) (2024) 299–315.
[59] P. Schöffski, A. Wozniak, S. Stacchiotti, P. Rutkowski, J.Y. Blay, L.H. Lindner, et al., Activity and safety of crizotinib in patients with advanced clear-cell sarcoma with

MET alterations: European Organization for Research and Treatment of Cancer phase II trial 90101 'CREATE', Ann. Oncol. 28 (12) (2017) 3000–3008.
[60] S. Garcia-Recio, T. Hinoue, G.L. Wheeler, B.J. Kelly, A.C. Garrido-Castro, T. Pascual, et al., Multiomics in primary and metastatic breast tumors from the AURORA US network finds microenvironment and epigenetic drivers of metastasis, Nat. Cancer 4 (1) (2023) 128–147.
[61] P. Priestley, J. Baber, M.P. Lolkema, N. Steeghs, E. de Bruijn, C. Shale, et al., Pan-cancer whole-genome analyses of metastatic solid tumours, Nature 575 (7781) (2019) 210–216.
[62] F. Martínez-Jiménez, P. Priestley, C. Shale, J. Baber, E. Rozemuller, E. Cuppen, Genetic immune escape landscape in primary and metastatic cancer, Nat. Genet. 55 (5) (2023) 820–831.
[63] A. Moorman, E.K. Benitez, F. Cambulli, Q. Jiang, A. Mahmoud, M. Lumish, et al., Progressive plasticity during colorectal cancer metastasis, Nature 637 (8047) (2025) 947–954.
[64] L. Kuett, A. Bollhagen, S. Tietscher, B. Sobottka, N. Eling, Z. Varga, et al., Distant metastases of breast cancer resemble primary tumors in cancer cell composition but differ in immune cell phenotypes, Cancer Res. 85 (1) (2025) 15–31.
[65] A. Pérez-González, K. Bévant, C. Blanpain, Cancer cell plasticity during tumor progression, metastasis and response to therapy, Nat. Cancer 4 (8) (2023) 1063–1082.
[66] D. Hanahan, R.A. Weinberg, Hallmarks of cancer: the next generation, Cell 144 (5) (2011) 646–674.
[67] R. Kalluri, The biology and function of fibroblasts in cancer, Nat. Rev. Cancer 16 (9) (2016) 582–598.
[68] T.H. Kim, D. Lee, H.J. Oh, I.H. Ham, T.T. Tran, Y. Lee, et al., Cancer-associated fibroblast-derived GAS6 increases resistance to chemotherapy through AXL/STAT3/ABCG1 in gastric cancer, Br. J. Cancer (2025).
[69] J. Ma, Y. Huang, J. Chen, Y. Li, R. Yao, X. Li, et al., FAP(+) fibroblasts orchestrate tumor microenvironment remodeling in renal cell carcinoma with tumor thrombus, Nat. Commun. 16 (1) (2025) 9387.
[70] A. Subramanian, N. Nemat-Gorgani, T.J. Ellis-Caleo, I.D.G.P. van, T.J. Sears, A. Somani, et al., Sarcoma microenvironment cell states and ecosystems are associated with prognosis and predict response to immunotherapy, Nat. Cancer 5 (4) (2024) 642–658.
[71] N. Kalakonda, M. Maerevoet, F. Cavallo, G. Follows, A. Goy, J.S.P. Vermaat, et al., Selinexor in patients with relapsed or refractory diffuse large B-cell lymphoma (SADAL): a single-arm, multinational, multicentre, open-label, phase 2 trial, Lancet Haematol 7 (7) (2020) e511–e522.
[72] S. Grosicki, M. Simonova, I. Spicka, L. Pour, I. Kriachok, M. Gavriatopoulou, et al., Once-per-week selinexor, bortezomib, and dexamethasone versus twice-per-week bortezomib and dexamethasone in patients with multiple myeloma (BOSTON): a randomised, open-label, phase 3 trial, Lancet 396 (10262) (2020) 1563–1573.